SIAM J. NUMER. ANAL.
Vol. 58, No. 2, pp. 962–987
© 2020 Society for Industrial and Applied Mathematics

Downloaded 05/07/20 to 128.193.164.203. Redistribution subject to SIAM license or copyright; see http://www.siam.org/journals/ojsa.php

APPROXIMATION OF SCALAR CONSERVATION LAW WITH HYSTERESIS*

MALGORZATA PESZYNSKA† AND RALPH E. SHOWALTER†

Abstract. We consider a scalar conservation law with hysteresis in which the flux function depends on the history of the evolution. The work is motivated by the need to account for hysteresis in important applications to transport with adsorption. To model hysteresis we use an auxiliary system of ODEs with constraints known as linear play combined with particularly chosen nonlinear truncation functions. A combination of these allows a quite general shape of hysteresis graph with piecewise linear primary and secondary scanning curves; this is distinct from the well-known Preisach model. We prove well-posedness of the model and stability of an explicit-implicit finite difference scheme. The challenge of history dependence requires auxiliary results in product spaces. Numerical results confirm convergence of linear or slower rate.

Key words. scalar conservation law, finite difference, hysteresis, history dependence, monotone graphs, evolution equations with constraints, nonlinear stability, differential inclusions, transport with adsorption, play hysteresis

AMS subject classifications. 65M12, 65M06, 35L65, 47J40, 34C55, 47H06, 35K55, 35L04

DOI. 10.1137/18M1197679

1. Introduction.

In this paper we propose and analyze a numerical scheme for the PDE

$$\frac{\partial}{\partial t}(a(u) + \mathcal{H}(u)) + \frac{\partial}{\partial x}(\alpha(u)) = F, \tag{1.1}$$

where $\mathcal{H}$ is a K-nonlinear play hysteresis operator to be defined and $a(\cdot)$, $\alpha(\cdot)$ are nonlinear monotone functions. Appropriate initial conditions, precise assumptions on $a(\cdot)$, $\alpha(\cdot)$, and definition of $\mathcal{H}$ will be given.

The problem (1.1) comes from the applications in transport with adsorption. Hysteresis in porous media and other applications and in particular in adsorption has been reported widely; we provide extensive motivation and references below. Without hysteresis, the amount adsorbed $\mathcal{H}(u)$ is a nonlinear increasing function of u determined experimentally; appropriate numerical schemes are well known, and analysis relies in particular on the Lipschitz continuity of $\mathcal{H}$. With hysteresis, the amount $\mathcal{H}(u)$ is represented by a different curve depending on the history of the process and whether the input u is increasing (adsorption) or decreasing (desorption); see Figure 1 for an illustration. Each of the bounding curves, also called (primary) scanning curves, is monotone. However, due to the history dependence, there is lack of Lipschitz continuity of $\mathcal{H}(u)$, and the usual analysis such as in [31, 30] does not apply.

To our knowledge, this paper presents the first result on the topic of numerical approximation of advective transport with hysteresis of structure (1.1). There are two main challenges we address. First, we *approximate* the hysteresis operator $\mathcal{H}$ so as to model realistic scanning curves with a finite number of piecewise linear segments. Second, we propose and analyze an approximation scheme for (1.1).

*Received by the editors July 2, 2018; accepted for publication (in revised form) December 2, 2019; published electronically March 12, 2020.
https://doi.org/10.1137/18M1197679
Funding: The work of the first author was partially supported by the National Science Foundation grants DMS-152273, DMS-1115827, and NSF-IRD 2019-20.
†Mathematics Department, Oregon State University, Corvallis, OR 97331-4605 (mpesz@math.oregonstate.edu, show@math.oregonstate.edu).

Copyright © by SIAM. Unauthorized reproduction of this article is prohibited.

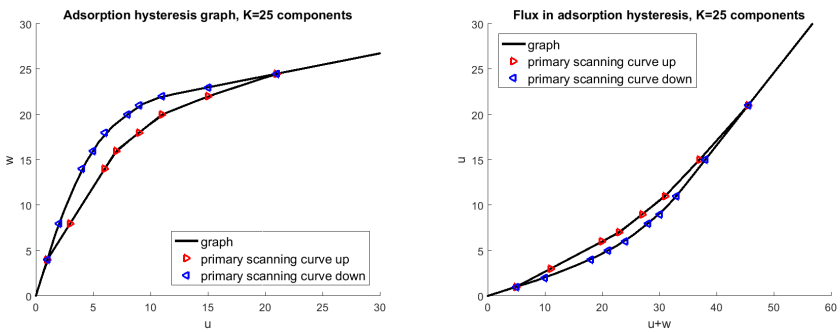

FIG. 1. *Left: K-nonlinear play hysteresis graph $(u, w) = (u, \mathcal{H}(u))$ with concave-concave scanning curves. Right: the "corresponding" flux function: the plot of $(u + w, u)$, with convex-convex scanning curves. The details of this example are in section* 3.2.

Toward the first goal, we build $w = \mathcal{H}(u)$ from K auxiliary evolution equations of nonlinear play type, which are coupled to the transport and contain the memory; we call it K-nonlinear play hysteresis. Our model has a structure similar to Preisach hysteresis, but our use of a finite number of smooth components makes it amenable to calibration; we defer the details to [43]. The model is easy to implement, and its numerical analysis is based on the classic monotone theory and solvers for problems under constraints. We analyze first the scheme for the auxiliary system of ODEs under constraints and develop intermediate results such as monotonicity and ordering properties. With these, we prove well-posedness for (1.1) in Banach space setting on a large product space $(L^1(0, l))^{K+1}$; the scalar problem is not m-accretive in u, even if the functions a and α reduce to the identity.

Second, we approximate the solutions to (1.1) with a numerical scheme which combines the explicit upwind discretization of the transport term with the implicit algorithm to resolve the (hysteresis) nonlinearity under $\frac{\partial}{\partial t}$. The algorithm is quite robust with the use of resolvent which is very intuitive. Our main result is the nonlinear stability of the scheme for $a = \mathrm{id}, \alpha = \mathrm{id}$ in the product space $(L^1(\mathbb{R}))^{K+1}$. The proof for $a \neq \mathrm{id}, \alpha \neq \mathrm{id}$ requires extra steps and follows next.

In numerical experiments we obtain in L^1 norm the usual $O(\sqrt{h})$ convergence rate for nonsmooth solutions and $O(h)$ rate for smooth solutions to (1.1). These rates agree with the abstract results for implicit semidiscrete finite difference schemes in [18, 46], but we emphasize that these do not apply directly to our scheme because the underlying operator in (1.1) is not m-accretive in u.

Finally, the special case when $a = \mathrm{id}, \alpha = \mathrm{id}$ reads

$$\frac{\partial}{\partial t}(u + \mathcal{H}(u)) + \frac{\partial}{\partial x}(u) = F. \tag{1.2}$$

When $\mathcal{H}$ includes only convex-concave pieces as in [44, 41], our numerical scheme allows stability estimates in a Hilbert space, with solutions to (1.2) considerably smoother than those for (1.1) and with experimentally observed $O(h)$ convergence rate. These seem superconvergent compared to those in [46] because the spatial operator is not a subgradient, even though $\mathcal{H}$ can be, with a proper choice of weighted space.

1.1. Related work and hysteresis models. Hysteresis is important in elastoplasticity and electromagnetics; see the classical monographs on modeling and analysis

Downloaded 05/07/20 to 128.193.164.203. Redistribution subject to SIAM license or copyright; see http://www.siam.org/journals/ojsa.php

Copyright © by SIAM. Unauthorized reproduction of this article is prohibited.

Downloaded 05/07/20 to 128.193.164.203. Redistribution subject to SIAM license or copyright; see http://www.siam.org/journals/ojsa.php

in [29, 59, 14, 33]. Hysteresis in capillary pressure is important in multiphase flow; see the recent analyses in [1, 2, 19, 21] and an extensive modeling review in [49].

Hysteresis in adsorption/desorption is a fundamental concept recognized in IUPAC classification, and considered important in the chemical engineering literature; see the highly cited experimental work [34, 15, 25] and recent large activity on getting the experimental data for $\mathcal{H}(u)$ for single and multicomponent adsorption hysteresis such as in [63]. See also applications to carbon sequestration and simulations of transport with multicomponent adsorption in coalbeds [45, 50]. Some authors postulate mechanisms at microscale which explain hysteresis and/or build statistical mechanics models [48, 62, 26, 38]. See [42, 35, 44, 27] for additional references.

In applied mathematics literature the differential models of hysteresis are set within the framework of monotone evolution equations and multivalued constraint graphs. The majority of papers focus on the well-known Preisach hysteresis model [33, p. 31] [59, p. 97] and parabolic equations; see, e.g., [32, 53]. In relation to our K-nonlinear play construction, Preisach model uses an infinite collection of building blocks, each of which has vertical and horizontal segments. In contrast, our model uses a sum of K building blocks with finite slopes which gives piecewise linear scanning curves; we come back to this in section 3.2. The sections of the hysteresis graph built with our model have sides that are not necessarily parallel; this makes our model a special case of the *generalized play* type of hysteresis [29, section 2], [59, p. 65]; we have not seen its full form, however, in a practical setting.

The modeling and well-posedness work closest to this paper is in [44, 27, 61], all on (1.2). Analysis of first-order PDEs with hysteresis in case (1.2) was considered in [44] as well as more recently in [60]; the latter model includes the K-nonlinear play case with $a = \mathrm{id}, \alpha = \mathrm{id}$ but seems difficult to approximate. In (1.1) the use of functions $a(\cdot)$, $\alpha(\cdot)$ provides additional modeling flexibility; e.g., it allows extensions to (compressible) gas adsorption.

1.2. Discrete schemes for scalar conservation laws, hysteresis, and multivalued monotone operators. Scalar conservation laws and their low-order numerical approximations are clearly a vast topic; we confine our citations here to the monographs [31, 30, 24, 57, 56]; other references to fundamental work can be found there, while higher-order schemes are out of our scope. Numerical analysis for problems with adsorption with $\mathcal{H} = 0$ was conducted primarily for diffusive transport; see [4, 5, 6, 7]. More recently, in [36] we pursued analysis of stability of a related problem of which inspired some analysis in the Hilbert space setting in section 6.5. However, we are not aware of any analysis of a fully discrete scheme for $\mathcal{H} \neq 0$ and in particular for (1.2) or (1.1) regardless of which hysteresis model is used.

Computations with hysteresis have been carried out before. The practical reservoir engineering models such as in [28] typically realize the history dependence and the constraints by explicitly coding the switching between the scanning curves. On the other hand, the algorithm in [55, 1.4, p. 41] for the "return-mapping theorem" in plasticity realizes the underlying constraint on the evolution but without the explicit use of resolvent. The hysteresis loops simulated with Preisach model are shown in [64, 23] but without analysis of the discrete scheme. Most recently, the Preisach model was used in [12] for a parabolic PDE modeling ferromagnetic hysteresis, but details of handling hysteresis are not given.

The fundamental work on finite differences for evolution equations with monotone multivalued operators is available in particular in [18, 17, 52, 13, 59, 3] and [46, 47, 40]. Numerical analysis closely related to ours is on the schemes for implicit evolution

Copyright © by SIAM. Unauthorized reproduction of this article is prohibited.

Downloaded 05/07/20 to 128.193.164.203. Redistribution subject to SIAM license or copyright; see http://www.siam.org/journals/ojsa.php

equations [8, 37] with various applications, while the work in [9] extends the method of "minimizing movements" by De Giorgi. An implicit time-discrete scheme is used in [61] as a step toward well-posedness proof of a model similar to (1.2) but with Preisach $\mathcal{H}(u)$.

Last but not least we note that a typical approach in the presence of multivalued graphs such as sgn^{-1} in [51, 61] or Heaviside function in [20] seems to be to use their regularization, which carries a modeling error. Our approach uses resolvent and thus avoids the modeling error as well as the difficulties associated with time stepping.

1.3. Plan of the paper. In section 2 we develop notation and preliminaries. In section 3 we define the K-nonlinear play hysteresis model $\mathcal{H}(u)$. In section 4 we consider an auxiliary system of ODEs which builds $\mathcal{H}(\cdot)$, and we develop auxiliary results. In section 5 we prove well-posedness of (1.1) in $(L^1)^{K+1}$ setting. In section 6 we define and analyze the numerical scheme for (1.1), and section 7 presents numerical experiments which show convergence rate $O(h)$ for a special case of $\mathcal{H}$ in (1.2) as well as $O(\sqrt{h})$ in the general case (1.1).

2. Discretization of ODEs with constraint graphs and overview of hysteresis.

We start with notation and preliminaries.

2.1. Assumptions and notation. In (1.1) we have $(x,t) \in \mathbb{R} \times (0,T]$ and consider $u(x,t) \in \mathbb{R}$. The time interval will be partitioned to $0 = t_0 < t_1 < \dots t_N = T$ with $t_n - t_{n-1} \le \tau$. For ease of exposition we use uniform time stepping and $t_n = n\tau$.

We will abbreviate and write $f = \mathrm{id}$ for the identity function $f(x) = x$. For real functions, we will abbreviate and say $f(\cdot)$ is monotone (strictly monotone) if f is monotone nondecreasing (increasing); this is consistent with the usual notions for operators. A real monotone function $f(\cdot)$ is maximal if $\mathrm{id} + f$ is onto $\mathbb{R}$.

The following assumptions will be used throughout:

$$a = \mathrm{id} + a_0, a_0(\cdot) \text{ is monotone, piecewise } \mathrm{C}^1, \text{ Lipschitz, } a_0(0) = 0, \tag{2.1a}$$

$$b(\cdot) \text{ is Lipschitz, monotone, piecewise } \mathrm{C}^1, \ b(0) = 0, \tag{2.1b}$$

$$\alpha(\cdot) \text{ is locally Lipschitz, strictly monotone, piecewise } \mathrm{C}^1, \ \alpha(0) = 0. \tag{2.1c}$$

These assumptions are sufficient for the analysis below.

In the definition of $\mathcal{H}$ we will use constraint graphs. For each nonempty closed interval $[\alpha, \beta] \in \mathbb{R}$ for $\alpha \le \beta$, the corresponding set-valued function or *constraint graph* is defined by

$$c_{\alpha,\beta}(s) = \begin{cases} (-\infty, 0] \text{ if } s = \alpha, \\ \{0\} \text{ if } \alpha < s < \beta, \\ [0, \infty) \text{ if } s = \beta \end{cases} \tag{2.2}$$

with the domain $\mathrm{Dom}\,(c_{\alpha,\beta}) = [\alpha, \beta]$. This is the subgradient $c_{\alpha,\beta} = \partial I_{[\alpha,\beta]}$ in $\mathbb{R} \times \mathbb{R}$ of the *indicator function* $I_{[\alpha,\beta]}$ for the interval $[\alpha, \beta]$: $I_{[\alpha,\beta]}(x) = 0$ if $x \in [\alpha, \beta]$ and $= +\infty$ otherwise. Clearly the range $\mathrm{Rg}(c) = \mathbb{R}$. For some $v \in \mathrm{Dom}(c)$ and some selection $c^* \in \mathbb{R}$ of the range of c, we will denote by $[v, c^*]$ an element of the graph of c.

In what follows we will omit the subscripts α, β and write $c(\cdot)$. We will also consider a family $c_k(\cdot)$ of graphs, each with an underlying $\mathrm{Dom}(c_k) = [\alpha_k, \beta_k]$.

We will also use the $\mathrm{sgn}(\cdot)$ graph and the $\mathrm{sgn}_0(\cdot)$ function. We recall $\mathrm{sgn}(x) = \mathrm{sgn}_0(x) = \frac{x}{|x|}$ if $x \ne 0$. In addition, $\mathrm{sgn}_0(0) = 0$, while $\mathrm{sgn}(0) = [-1, 1]$.

Copyright © by SIAM. Unauthorized reproduction of this article is prohibited.

Downloaded 05/07/20 to 128.193.164.203. Redistribution subject to SIAM license or copyright; see http://www.siam.org/journals/ojsa.php

2.2. Abstract setting. An initial-boundary-value problem for (1.1) will be framed as an abstract Cauchy problem posed on a Banach space X:

$$\tfrac{d}{dt}\psi(t) + A(\psi(t)) \ni f(t), \quad 0 < t \le T, \quad \psi(0) = \psi_{init}. \tag{2.3}$$

In this section we recall some notation and preliminaries for (2.3). See [52, 3, 59, 13] for details. In particular, the inclusion symbol "$\ni$" indicates that A may be multivalued; we address this below. We recall that an *operator* A on a Banach space X is a subset of $X \times X$, and we identify A with its graph, so $A(x) = \{y : [x, y] \in A\}$ for $x \in \mathrm{Dom}(A)$. The operator A is *accretive* if $\|x_1 - x_2\| \le \|(x_1 + \mu y_1) - (x_2 + \mu y_2)\|$ for all $\mu > 0$, $[x_1, y_1]$, $[x_2, y_2] \in A$ and *m-accretive* if also $\mathrm{Rg}\,(I + A) = X$. Then it follows that $\mathrm{Rg}\,(I + \mu A) = X$ for every $\mu > 0$.

2.3. Discrete scheme and the solutions to (2.3). We shall apply the following seminal result on nonlinear evolution equations which employs a discrete scheme.

THEOREM 2.1 ([11], [17], [18] [52, IV.8]). *If A is accretive in the Banach space X, $f \in L^1(0, T; X)$, and $\psi_{init} \in \overline{\mathrm{Dom}\,(A)}$, then there is at most one C^0-solution of the initial-value problem* (2.3). *If additionally*

$$\overline{\mathrm{Dom}\,(A)} + \mu\,\bar{f} \subset \mathrm{Rg}\,(I + \mu A) \text{ for every } \mu > 0 \text{ and constant } \bar{f} \in \mathrm{Rg}\, f(\cdot), \tag{2.4}$$

then there exists a unique C^0-solution of (2.3).

We recall that the C^0-solution $\psi \in C([0, T], X)$ is a uniform limit of step functions $\Psi_\tau(t)$ (equal ψ^n if $t \in (t_{n-1}, t_n]$), which satisfy the difference equations

$$\tfrac{\psi^n - \psi^{n-1}}{t_n - t_{n-1}} + A(\psi^n) \ni f_n, \quad 1 \le n \le N, \tag{2.5}$$

where f_n is an approximation to $f(t_n)$ chosen so that the corresponding step function $F_\tau(t)$ satisfies $\|f - F_\tau\|_{L^1(0,T)} \to 0$ as $\tau \to 0$. Usually $f_n = f(t_n)$ so that (2.5) is fully implicit.

The approximation ψ^n is determined uniquely by

$$\psi^n = (I + (t_n - t_{n-1})A)^{-1}(\psi^{n-1} + (t_n - t_{n-1})f_n), \quad 1 \le n \le N. \tag{2.6}$$

The operator $(I + \lambda A)^{-1}$ for $\lambda > 0$ is the *resolvent* of A. We emphasize that the resolvent is a contraction; hence, ψ^n is unique, and the symbol $=$ in (2.6) replaces $\ni$ in (2.5).

A sufficient condition for (2.4) is that A be m-accretive. The more general range condition (2.4) implies that the implicit difference equation (2.5) can be resolved successively to obtain ψ_n, and then the Crandall–Evans proof establishes the uniform convergence of $\Psi_\tau(t)$ to $\psi(t)$. The more general range condition (2.4) is needed in section 5. We refer to [22, 52] for expositions of the semigroup theory and various applications to initial-boundary-value problems for PDEs. In particular, a range condition more general than (2.4) is given in [17, Remark 4.17].

While we do not exploit the abstract results directly, the a priori and a posteriori analysis of the estimates for the error $\psi(t) - \Psi_\tau(t)$ depends on the functional setting and on the properties of operator A. In a Banach space X when A is m-accretive, the error $\|\,\psi(t) - \Psi_\tau(t)\,\|_X$ is $O(\sqrt{\tau})$. The results are stronger when X is a Hilbert space and when A is a subgradient. Then [46, section 6] the rate is $O(\tau)$ provided $\psi_{init} \in \mathrm{Dom}(c)$, $f \in H^1(0, T; H)$. See also [40] for a posteriori analysis on nonuniform grid in Hilbert spaces. In all these results $f_n = f(t_n)$. In our algorithm $f_n = f(t_{n-1})$; in section 7 we confirm these rates for (1.1) and (1.2) for a fully discrete scheme.

Copyright © by SIAM. Unauthorized reproduction of this article is prohibited.

Downloaded 05/07/20 to 128.193.164.203. Redistribution subject to SIAM license or copyright; see http://www.siam.org/journals/ojsa.php

2.4. ODE with constraint graph. Now we recall additional information on (2.3) when $X = \mathbb{R}$ and $A = c$ with c defined in (2.2). We employ here Hilbert space setting with the meaning of inclusion "$\ni$" elucidated clearly in [13]. We have

$$\tfrac{d}{dt}\psi(t) + c(\psi) \ni f(t), \quad \psi(0) = \psi_{init}. \tag{2.7}$$

Here the term $c(\psi)$ plays the role of the "penalty functional" or of Lagrange multiplier for the constraint $\psi \in \mathrm{Dom}\,(c) \equiv [\alpha, \beta]$. When α, β are $-\infty$ or ∞, respectively, we have one-sided constraint. The unconstrained case is when $\mathrm{Dom}\, c = \mathbb{R}$. The case when $\alpha = \beta$ and $\mathrm{Dom}\, c = \{\alpha\}$ enforces $\psi = \alpha = \beta$.

The constraint graph $c(\cdot)$ has the special property which we exploit repeatedly.

Remark 2.2. For any $\lambda > 0$, we have the equality of sets $c(s) = \lambda c(s)$. In particular, we have that the resolvent $R = (I + \lambda c)^{-1} = (I + c)^{-1} : \mathbb{R} \to [\alpha, \beta]$ is a monotone piecewise C^1 function with unit Lipschitz constant. However, for a given $c^* \in c(\cdot)$ and $\lambda \neq 1$, we do not have equality of λc^* and c^* unless $c^* = 0$. On the other hand, in finite difference setting, the solution ψ^n satisfies $\psi^n + \tau c(\psi^n) \ni \psi^{n-1}$. We will refer to c^* always as to the selection out of τc.

With this, on a uniform time grid with time step τ the finite difference approximations ψ^n defined in (2.6) are given by using the resolvent $R(\cdot) : \mathbb{R} \to [\alpha, \beta] = \mathrm{Dom}(c)$:

$$\psi^n = R(\tau f_n + \psi^{n-1}), \quad R(s) = \begin{cases} \alpha \text{ if } s < \alpha, \\ s \text{ if } \alpha \le s \le \beta, \\ \beta \text{ if } s > \beta. \end{cases} \quad s \in \mathbb{R}, \tag{2.8}$$

We can also return to the meaning of inclusion (2.5). We have that $\psi^n = v$, where v solves the stationary problem $v + c(v) \ni f = \tau f_n + \psi^{n-1}$. (In this paper instead of $v + c(v) \ni f$ we favor the notation $v + c^* = f,\ c^* \in c(v)$.) In the Hilbert space setting we know [39] that v is the (unique) minimizer of the convex l.s.c. function $\mathcal{G}(\psi) = \frac{1}{2} \parallel \psi - f \parallel_X^2 + I_{[\alpha,\beta]}(\psi)$ over X or, equivalently, of $\frac{1}{2} \parallel \psi - f \parallel_X^2$ over $\mathrm{Dom}(c)$. While $v \in \mathrm{Dom}(c)$ is unique, in general, $v + c(v)$ is a set. However, once v is determined, the selection c^* is unique.

3. Hysteresis models. We first describe various hysteresis functionals of *play* type, from the simplest to the more general. We illustrate with examples; the figures are produced with an ODE solver to be described in the companion paper [43].

3.1. Linear play and *K*-linear play. The most basic hysteresis functional is called *linear play* [59, p. 63]. In this model, the output $v(t)$ follows the input $u(t)$ within a fixed constraint on their maximum distance from each other. The input-output graph consists of parallel lines of unit slope for which the output $v(t)$ is increasing on the right, decreasing on the left, and constant between them. The dependence of v on u is highly nonlinear; the name "linear play" refers only to the affine boundaries of the constraint set. If the constraint interval is $[\alpha, \beta]$, the corresponding maximal monotone constraint graph $c = c_{[\alpha,\beta]}$ determines the well-posed initial-value problem

$$\tfrac{d}{dt}v(t) + c(v(t) - u(t)) \ni 0\,, \quad v(0) = v_{init} \in u_{init} + [\alpha, \beta]\,. \tag{3.1}$$

Note that the initial data must be chosen consistent with the constraint. The solution $v(t) = \mathcal{H}(u)(t)$ is the *linear play*. The output $v(\cdot)$ starts at $v(0) = v_{init}$, then, while the input $u(\cdot)$ increases, $v(t) = (u(t) - (v_{init} - \alpha))^+ + v_{init}$. If $u(\cdot)$ decreases, then $v(t) = (u(t) - (v_{init} - \beta))^- + v_{init}$. See illustration in Figure 2, left.

Copyright © by SIAM. Unauthorized reproduction of this article is prohibited.

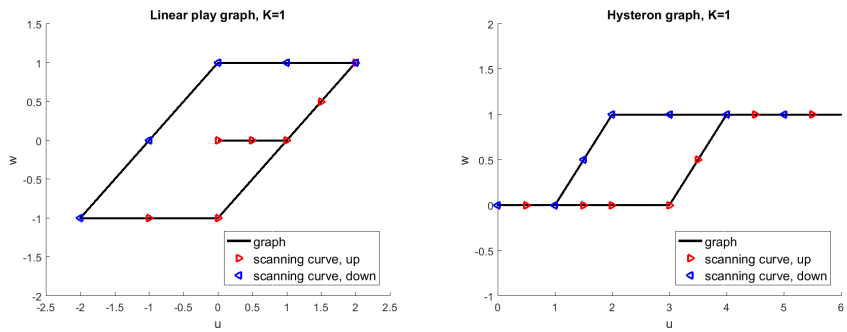

FIG. 2. *Elementary graphs used in the construction of $\mathcal{H}(u)$ graph; shown are the upward and downward scanning curves. Left: linear play with $w = \bar{v}_{[-1,1]}$. We show the graph obtained when u oscillates between -2 and 2 starting from 0 to 2. Right: hysteron example $w = b^1(\bar{v}_{[1,3]})$.*

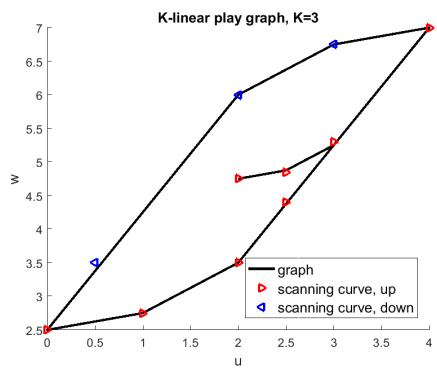

FIG. 3. *Example of K-linear play $\mathcal{H}(u)$ graph from [44] given as $w = \frac{1}{4}\bar{v}_{[0,0]} + \frac{1}{2}\bar{v}_{[0,1]} + \bar{v}_{[0,2]}$. Notice it has convex-concave sides unlike those shown in Figure 1. The scanning curves are followed first starting from $u = 2$ and increasing to 4.*

In practice, when calibrating the examples, it is most convenient to work with the constraint $v + \alpha \le u \le v + \beta$, i.e., $-\beta \le v - u \le -\alpha$. Define $\bar{v}_{\alpha,\beta}(u) = v$, where v is the unique solution to the *constraint equation*

$$\frac{dv}{dt} + c_{-\beta,-\alpha}(v - u) \ni 0, \quad v(0) = v_{init} \in u(0) + [-\beta, -\alpha]. \tag{3.2}$$

When the constraint interval is a single point, we have $\bar{v}_{\alpha,\alpha}(u) = u - \alpha$.

In this paper we call the hysteresis operators composed of a sum of K positive multiples of linear play functionals over a collection of constraint intervals the *K-linear play* model. The graph is constrained by an increasing convex function on the right and a decreasing concave function on the left. The convex-concave character arises from the fact that the linear play functionals are not truncated, so the *slope* of their sum is monotone with respect to the input. That is, once a constraint is active, it remains active until the input reverses direction. A collection of intervals $[\alpha_k, \beta_k]$ and positive numbers μ_k, $1 \le k \le K$, determine a K-linear play hysteresis functional $\mathcal{H}(u) = \sum_{k=1}^{K} \mu_k\, \bar{v}_{\alpha_k,\beta_k}(u)$. We shall write this in the form $\mathcal{H}(u) = \sum_{k=1}^{K} b_k(\bar{v}_k)$, where $b_k = \mu_k$ id and $\bar{v}_k = \bar{v}_{\alpha_k,\beta_k}(u)$. See Figure 3 for an example.

3.2. Nonlinear play. More general are the hysteresis functionals determined by translates of a maximal monotone shape function $b(v)$. Here the output is increasing

Copyright © by SIAM. Unauthorized reproduction of this article is prohibited.

Downloaded 05/07/20 to 128.193.164.203. Redistribution subject to SIAM license or copyright; see http://www.siam.org/journals/ojsa.php

Downloaded 05/07/20 to 128.193.164.203. Redistribution subject to SIAM license or copyright; see http://www.siam.org/journals/ojsa.php

on the right as $w = b(u-\beta)$, decreasing on the left along $w = b(u-\alpha)$, and constant between them. These functionals are called *nonlinear play* [59, p. 63], and they can be obtained from the input $u(\cdot)$ by the formula $w(t) = \mathcal{H}(u)(t) = b(\bar{v}_{\alpha,\beta}(t))$ and the constraint equation (3.2). Nonlinear play hysteresis serves a fundamental role for the construction of hysteresis models below. For our construction of $\mathcal{H}$, let $b^1(u) = u^+ - (u-1)^+$ denote the *unit truncation function*. Then we define the *unit step* to be $b^1(\bar{v}_{\alpha,\beta}(u))$, where $\bar{v}_{\alpha,\beta}(u)$ is the solution of (3.2). See the example in Figure 2, right, where a simple so-called *hysteron* $w = b^1(\bar{v}_{[1,3]})$ is shown.

The *K-nonlinear play* hysteresis functionals are sums of K-nonlinear play hysteresis functionals over a collection of constraint intervals

$$\mathcal{H}(u) = \sum_{k=1}^{K} \mu_k\, b^1\big(\bar{v}_{\alpha_k,\beta_k}(u)\big) = \sum_{1}^{K} b_k(\bar{v}_k),$$

where we set $b_k(\cdot) = \mu_k b^1(\cdot)$ and $\bar{v}_k = \bar{v}_{\alpha_k,\beta_k}(u)$ is the linear play (3.2).

Finally, we need the *scaled truncation function* $b_{A,B}(u) = (u-A)^+ - (u-B)^+$ for $A < B$. These functions are useful to add a fixed slope on a designated interval to another function or functional.

Our final example is the K-nonlinear play model of an adsorption isotherm shown in Figure 1. For shorthand, define $\gamma_{\alpha,\beta} = b^1\big(\bar{v}_{\alpha,\beta}(u)\big)$. With this, we set

$$\begin{aligned} w = \mathcal{H}(u) = 4\, b_{0,1}(u) &+ (2\gamma_{1,1} + 2\gamma_{1,2}) \\ &+ (\gamma_{2,3} + \gamma_{3,3} + \gamma_{2,4} + \gamma_{3,4} + \gamma_{2,5} + \gamma_{3,5}) \\ + 2\gamma_{4,6} + (\gamma_{5,7} + \gamma_{5,8}) &+ (\gamma_{6,9} + \gamma_{7,10}) + \tfrac{1}{4}(\gamma_{8,11} + \gamma_{8,12} + \gamma_{8,13} + \gamma_{8,14}) \\ &+ \tfrac{1}{6}(\gamma_{9,15} + \gamma_{9,16} + \gamma_{9,17} + \gamma_{10,18} + \gamma_{10,19} + \gamma_{10,20}) + \tfrac{1}{4} b_{11,101}(u). \end{aligned} \tag{3.3}$$

At this point we remark that Preisach hysteresis functionals are obtained by using the $\mathrm{sgn}(\cdot)$ graph in place of $b^1(\cdot)$, and integrals over $\{(\alpha,\beta) : \alpha < \beta\}$ in $\mathbb{R}^2$ instead of a finite sum [33, p. 31], [59, p. 97]. In our model we approximate $\mathrm{sgn}(\cdot)$ by the truncation $\frac{1}{\varepsilon} b_{-\varepsilon,\varepsilon}(\cdot)$ with $\varepsilon \to 0$, and we use finite sums; this provides practical piecewise linear scanning curves.

4. Analysis of a discrete scheme for ODE system with hysteresis. We develop and analyze now an algorithm for the approximation to the solutions $(u(t), w(t))$ to an evolution system driven by some external input $f(t)$ with $w = \mathcal{H}(u)$. The results are fundamental for the analysis in section 5 and stability analysis for a scheme for (1.1) we develop in section 6.

We consider the K-nonlinear play model

$$\tfrac{d}{dt}(a(u) + w) = f(t), \tag{4.1a}$$

$$w = \mathcal{H}(u) = \sum_k b_k(v_k),\ \ \tfrac{d}{dt} v_k + c_k^* = 0,\ \ c_k^* \in c_k(v_k - u(t))\ \ \forall k. \tag{4.1b}$$

The system is complemented with initial conditions

$$u(0) = u_{init},\ \ v_k(0) = v_{k,init} \in u_{init} + \mathrm{Dom}\,(c_k). \tag{4.1c}$$

In approximation, we consider a sequence of discrete times $0 = t_0, t_1, \dots t_N = T$ with uniform time step $\tau = t_n - t_{n-1}$. We seek the approximations $u^n \approx u(t_n)$, $w^n \approx w(t_n)$, $v_k^n \approx v_k(t_n)$.

Copyright © by SIAM. Unauthorized reproduction of this article is prohibited.

Downloaded 05/07/20 to 128.193.164.203. Redistribution subject to SIAM license or copyright; see http://www.siam.org/journals/ojsa.php

4.1. Scheme for linear play. We first discretize the single constraint equation, one part of (4.1b) or (3.1), as the basic ingredient of the linear play hysteresis model

$$\tfrac{d}{dt}v(t) + c^* = 0, c^* \in c(v-u). \tag{4.2}$$

An implicit finite difference scheme (2.5) for (4.2) is defined as follows:

$$\tfrac{1}{\tau}(v^n - v^{n-1}) + c^* = 0, \quad c^* \in c(v^n - u^n). \tag{4.3}$$

Remark 4.1. In what follows we frequently take advantage of an equivalent form of (4.3) obtained via writing $v^n + \tau c^* = v^{n-1}$, subtracting u^n from both sides, and applying the resolvent (2.8) to get

$$v^n = u^n + R(v^{n-1} - u^n) = \begin{cases} u^n + \alpha, & v^{n-1} - u^n \le \alpha, \\ v^n, & \alpha < v^{n-1} - u^n < \beta, \\ u^n + \beta, & v^{n-1} - u^n \ge \beta. \end{cases} \tag{4.4}$$

4.2. Fully implicit scheme for the system (4.1). We set $f^n = f(t_n)$ or some other consistent value, e.g., $f^n = f(t_{n-1})$, and define the scheme, using (4.4),

$$a(u^n) - a(u^{n-1}) + w^n - w^{n-1} = \tau f^n, \tag{4.5a}$$

$$w^n = \sum_k b_k(v_k^n), \; v_k^n = R_k(v_k^{n-1} - u^n) + u^n \;\; \forall k. \tag{4.5b}$$

We will also set

$$u^0 = u_{init}, \quad v_k^0 = v_{k,init} \; \forall k. \tag{4.5c}$$

Note that given u^n, each $v_k^n, k = 1, \dots K$ can be found independently using the resolvent R_k corresponding to c_k, and we calculate $w^n = \sum_k b_k(v_k^n)$. Of course, the system (4.5) is still (nonlinearly) coupled since (4.5a) depends on w calculated in (4.5b). In practice, this system is solved by iteration: We plug in all of (4.5b) to (4.5a), solve it for u^n, and once u^n is found, we evaluate w^n. The solvability of the system will be proven in section 4.3. In section 4.4 we also prove auxiliary results to be used later.

Remark 4.2. The scheme (4.5) is easy to implement with, e.g., a Newton solver. Since the Jacobian is only semismooth, one cannot expect better than superlinear convergence [58], but in practice the convergence is quick due to the piecewise linear character of nonlinearities.

4.3. Solvability and stability of the scheme (4.5). We start with several auxiliary lemmas.

LEMMA 4.3. *Let $b(\cdot)$ satisfy* (2.1b). *If $v + c^* = g, c^* \in c(v-u)$, then $b(v) + c^{**} = b(g), c^{**} \in c(v-u)$, where c^* and c^{**} are possibly different selections out of $c(v-u)$.*

Proof. This follows directly from the observation that $b(v) - b(g)$ is positive or negative when the same holds for $v - g$. ∎

LEMMA 4.4. *Let $a(\cdot)$ be a strongly monotone function satisfying* (2.1a), *$(b_k(\cdot))_k$ satisfy* (2.1b) *and $(c_k)_k$ be the collection of constraint graphs. Let also $f, \bar{f} \in \mathbb{R}$ be given with the corresponding solutions $u, (v_k)_k$ and $\bar{u}, (\bar{v}_k)_k$ to the systems*

$$a(u) + \sum_k b_k(v_k) = f + \sum_k b_k(g_k), \; v_k + c_k^* = g_k, \; c_k^* \in c_k(v_k - u) \; \forall k, \tag{4.6a}$$

$$a(\bar{u}) + \sum_k b_k(\bar{v}_k) = \bar{f} + \sum_k b_k(\bar{g}_k), \; \bar{v}_k + \bar{c}_k^* = \bar{g}_k, \; \bar{c}_k^* \in c_k(\bar{v}_k - \bar{u}) \; \forall k. \tag{4.6b}$$

Copyright © by SIAM. Unauthorized reproduction of this article is prohibited.

Downloaded 05/07/20 to 128.193.164.203. Redistribution subject to SIAM license or copyright; see http://www.siam.org/journals/ojsa.php

Then these solutions satisfy the comparison estimate

$$|a(u)-a(\bar{u})|+\sum_k |b_k(v_k)-b_k(\bar{v}_k)|\leq|f-\bar{f}|+\sum_k |b_k(g_k)-b_k(\bar{g}_k)| \tag{4.7}$$

and the corresponding stability estimate

$$|a(u)|+\sum_k |b_k(v_k)|\leq|f|+\sum_k |b_k(g_k)|\,. \tag{4.8}$$

Proof. First we provide the proof for $a=\mathrm{id}$, $K=1$. From Lemma 4.3 we find, after making appropriate selections of c^{**}, $\bar{c}^{**}$ in (4.6), that

$$\begin{aligned} u-c^{**}=f,\ b(v)+c^{**}=b(g),\ c^{**}\in c(v-u),\\ \bar{u}-\bar{c}^{**}=\bar{f},\ b(\bar{v})+\bar{c}^{**}=b(\bar{g}),\ \bar{c}^{**}\in c(\bar{v}-\bar{u}). \end{aligned}$$

Subtracting the respective equations of each line, we obtain

$$u-\bar{u}-(c^{**}-\bar{c}^{**})=f-\bar{f},\ b(v)-b(\bar{v})+c^{**}-\bar{c}^{**}=b(g)-b(\bar{g}).$$

Multiplication of respective components by $\sigma_u=\mathrm{sgn}_0(u-\bar{u})$ and $\sigma_v=\mathrm{sgn}_0(v-\bar{v})$ yields, upon adding these together and observing that $\sigma_v\in\mathrm{sgn}(b(v)-b(\bar{v}))$,

$$|u-\bar{u}|+|b(v)-b(\bar{v}|+(c^{**}-\bar{c}^{**})(\sigma_v-\sigma_u)\leq|f-\bar{f}|+|b(g)-b(\bar{g})|\,.$$

To see the third term is positive, note that

- $v-\bar{v}>u-\bar{u}$ implies $v-u>\bar{v}-\bar{u}$, so both factors $(c^{**}-\bar{c}^{**})$ and $(\sigma_v-\sigma_u)$ are positive;
- $v-\bar{v}<u-\bar{u}$ implies $v-u<\bar{v}-\bar{u}$, so both factors are negative;
- $v-\bar{v}=u-\bar{u}$ implies the right factor $(\sigma_v-\sigma_u)$ is zero.

This yields

$$|u-\bar{u}|+|b(v)-b(\bar{v})|\leq|f-\bar{f}|+|b(g)-b(\bar{g})|, \tag{4.9}$$

which is (4.7) for the case $K=1$, $a=\mathrm{id}$.

For $K>1$ and the solutions of (4.6), Lemma 4.3 gives selections $\{c_k^{**}\},\{\bar{c}_k^{**}\}$ for which we have

$$\begin{aligned} a(u)-\sum_k c_k^{**}=f,\ b_k(v_k)+c_k^{**}=b_k(g_k),\ c_k^{**}\in c_k(v_k-u),\ 1\leq k\leq K,\\ a(\bar{u})-\sum_k \bar{c}_k^{**}=\bar{f},\ b_k(\bar{v}_k)+\bar{c}_k^{**}=b_k(\bar{g}_k),\ \bar{c}_k^{**}\in c_k(\bar{v}_k-\bar{u}),\ 1\leq k\leq K. \end{aligned}$$

Subtract corresponding equations; multiply by $\sigma_0=\mathrm{sgn}_0(u-\bar{u})$ and $\sigma_k=\mathrm{sgn}_0(v_k-\bar{v}_k)$, respectively; and add the products to obtain as before

$$\begin{aligned} |a(u)-a(\bar{u})|+\sum_k |b_k(v_k)-b_k(\bar{v}_k)|+\sum_k(c_k^{**}-\bar{c}_k^{**})(\sigma_k-\sigma_0)\\ \leq|f-\bar{f}|+\sum_k |b_k(g_k)-b_k(\bar{g}_k)| \end{aligned}$$

due to monotonicity of $a(\cdot)$ and each $b_k(\cdot)$ and because the third term consists of nonnegative summands. ∎

Copyright © by SIAM. Unauthorized reproduction of this article is prohibited.

Downloaded 05/07/20 to 128.193.164.203. Redistribution subject to SIAM license or copyright; see http://www.siam.org/journals/ojsa.php

PROPOSITION 4.5 (solvability and stability of (4.5) for nonlinear play). *Assume* (2.1a)–(2.1b). *Then the scheme* (4.5) *for* (4.1) (i) *has a unique solution and* (ii) *is stable. Namely, we have*

$$|a(u^n)| + \sum_k |b_k(v_k^n)| \leq \tau\,|f^n| + |u^{n-1}| + \sum_k |b_k(v_k^{n-1})|\,. \tag{4.10}$$

Proof. First we rewrite (4.5) so as to apply Lemma 4.4. Recall also Remark 4.1. For each k, we have $v_k^n + c_k^* = v_k^{n-1}$ with $c_k^* \in c_k(v_k^n - u^n)$. Thus,

$$a(u^n) + \sum_k b_k(v_k^{n-1}) = \tau f^n + \sum_k b_k(v_k^{n-1}),\ v_k^n + c_k^* = v_k^{n-1}, c_k^* \in c_k(v_k^n - u^n).$$

This is exactly the form in which Lemma 4.4 applies after we suppress the superscripts n on u^n, v_k^n and recognize $f = \tau f^n + u^{n-1}$, $g_k = v_k^{n-1}$.

To prove uniqueness, we apply the comparison part of Lemma 4.4. Stability follows also immediately.

To prove existence of solutions, we substitute the solutions v_k^n to (4.5b) in (4.5a), so that u^n satisfies

$$G(u^n) = a(u^n) + \sum_k b_k\left(u^n + R_k(v_k^{n-1} - u^n)\right) = \tau f^n + u^{n-1} + \sum_k b_k(v_k^{n-1}).$$

Now the left-hand-side function $G(\cdot)$ is strongly monotone with range $\mathbb{R}$; thus, for any right-hand side there is a unique solution u^n. Once we have u^n, we calculate v_k^n and w^n from (4.5b). ∎

4.4. Additional properties. The next result exploits the fact that (4.1) is solved on $\mathbb{R}^{K+1}$, and thus the components of the solutions enjoy certain ordering and "conservation" properties. In particular, while $|a(u^n) - a(u^{n-1}) + w^n - w^{n-1}| = \tau\,|f^n|$ holds trivially from (4.5a), we can prove a more refined result separating the two components $a(u)$ and w.

PROPOSITION 4.6 (properties of the solutions to (4.5) at every n). *The solution to* (4.5) *satisfies*

$$|a(u^n) - a(u^{n-1})| + \sum_k |b_k(v_k^n) - b_k(v_k^{n-1})| = \tau\,|f^n|\,. \tag{4.11}$$

Proof. As part of the proof below, we need to ensure that each $v_k^{n-1} \in u^{n-1} + \mathrm{Dom}(c_k)$. At $n = 1$ this follows from (4.5c). For $n > 1$ we have (4.4).

Now, to prove (4.11), we first consider $a = \mathrm{id}$.

The main ingredient of the proof is to demonstrate certain ordering properties. We show that

$$f^n \geq 0 \implies u^n - u^{n-1} \geq 0 \ \ \&\ \ b_k(v_k^n) \geq b_k(v_k^{n-1})\ \forall k. \tag{4.12}$$

The case $f^n \leq 0$ implies an analogous ordering $u^n - u^{n-1} \leq 0$ with each $b_k(v_k^n) \leq b_k(v_k^{n-1})$. From these ordering statements, the identity (4.11) follows immediately by applying $|\cdot|$ in (4.5a).

To prove (4.12), we show first that the sign of each $v_k^n - v_k^{n-1}$, where v_k^n solves (4.5b), is the same as the sign of $u^n - u^{n-1}$. To this aim for each k we define

$$r_k(s) = s + R_k(-s) = \begin{cases} s + \alpha_k, & s \geq -\alpha_k, \\ 0, & -\beta_k \geq s \geq -\alpha_k, \\ s + \beta_k, & s \leq -\beta_k, \end{cases}$$

Copyright © by SIAM. Unauthorized reproduction of this article is prohibited.

Downloaded 05/07/20 to 128.193.164.203. Redistribution subject to SIAM license or copyright; see http://www.siam.org/journals/ojsa.php

which is a monotone nondecreasing function. (In fact, it is the Yosida approximation c_λ to c with $\lambda = 1$.) From (4.5b) we see that

$$v_k^n - v_k^{n-1} = r_k(u^n - v_k^{n-1}). \tag{4.13}$$

Now, if $u^n \geq u^{n-1}$, this implies $r_k(u^n - v_k^{n-1}) \geq r_k(u^{n-1} - v_k^{n-1}) = 0$ since we assumed $v_k^{n-1} - u_k^{n-1} \in \mathrm{Dom}(c)$. By (4.13) we infer $v_k^n - v_k^{n-1} \geq 0$. In turn, if $u^n \leq u^{n-1}$, we obtain $v_k^n \leq v_k^{n-1}$ by analogous reasoning. We obtain analogous statements on the sign of $b_k(v_k^n) - b_k(v_k^{n-1})$ from monotonicity of each $b_k(\cdot)$.

Next we analyze the solutions to (4.5a) when $f^n \geq 0$. (Case $f_n \leq 0$ is analogous). We rewrite (4.5a) to be solved for $\tilde{u} = u^n - u^{n-1}$ and $\tilde{w}_k = b_k(v_k^n) - b_k(v_k^{n-1})$:

$$\tilde{u} + \sum_k \tilde{w}_k = \tau f^n.$$

Since the sign of $\tilde{u}$ is the same as the sign of each $\tilde{w}_k$, this scalar equation has a nonnegative solution $\tilde{u}$ exactly when $f^n \geq 0$. Thus, (4.12) follows, and this completes the proof for $a = \mathrm{id}$.

When $a \neq \mathrm{id}$, the proof follows analogously, since $a(\cdot)$ is strictly monotone. ∎

5. Well-posedness of PDE with K-nonlinear play hysteresis. Our goal here is to establish the well-posedness of initial-boundary-value problems for (1.1) in the form

$$\tfrac{\partial}{\partial t}\left(a(u(t)) + w(t)\right) + \tfrac{\partial}{\partial x}\alpha(u(t)) = F(t)\,, \tag{5.1a}$$

$$w(t) = \mathcal{H}(u(t)) = \sum_{k=1}^{K} b_k(v_k(t)),\ \tfrac{d}{dt}v_k(t) + c_k^*(t) = 0, c_k^*(t) \in c_k(v_k(t) - u(t)), \tag{5.1b}$$

$$u(x,0) = u_{init}(x), \quad u(0,t) = 0, \quad v_k(x,0) = v_{k,init}(x). \tag{5.1c}$$

The semigroup treatment of the conservation law with $\mathcal{H}(u) = 0$ is certainly not new [16, 10, 44, 52, 54, 60, 61]. Initial-boundary-value problems for such scalar conservation laws with $\mathcal{H}(u) = 0$ are well known to possess many weak solutions from which the *entropy* solution is the *correct* choice, and this solution can be obtained as the C^0-solution given by semigroup theory in L^1. See [16], where any spatial dimension N is permitted and the relation with Kruzkov's entropy solution is established. Here we treat the case $N = 1$; see [54], where $\alpha(\cdot)$ is a maximal monotone relation. Examples and references of scalar conservation laws with hysteresis are given in [59].

THEOREM 5.1. *Assume that $a(\cdot)$, $\alpha(\cdot)$ and each $b_k(\cdot)$ satisfy the assumptions* (2.1). *The operator A is defined by $A(u) = \frac{d}{dx}\alpha(u) \in L^1(0,\ell)$ with the domain* $\mathrm{Dom}(A)$ *consisting of those $u \in L^1(0,\ell)$ for which $\alpha(u) \in W^{1,1}(0,\ell)$ and $\alpha(u(0)) = 0$. Assume also $u_{init} \in \mathrm{Dom}\,(A)$ and*

$$v_{k,init} \in u_{init} + \mathrm{Dom}\,(c_k(\cdot)),\ 1 \leq k \leq K \tag{5.2}$$

and that $F \in L^1(0,T,L^1(0,\ell))$. Then there is a unique C^0-solution of the system (5.1) *with the K-nonlinear play hysteresis functional $\mathcal{H}(u) = \sum_{k=1}^K b_k(v_k)$.*

Proof. First we rewrite (5.1) as a system (2.3).

The operator A is m-accretive on $L^1(0,\ell)$ [54]. Define the operator $\mathbb{A}$ on the space $L^1(0,\ell) \times L^1(0,\ell)^K$ by $\mathbb{A}(a,(b_k)_k) \ni (f,(g_k)_k)$ if there exist functions $u \in \mathrm{Dom}(A)$, $v_k \in u + \mathrm{Dom}(c_k(\cdot))$ such that $a = a(u)$, $b_k = b_k(v_k)$, $g_k \in c_k(v_k - u)$, and

Copyright © by SIAM. Unauthorized reproduction of this article is prohibited.

$f + \sum_{k=1}^K g_k = A(u)$. All of the functions a, b_k, u, v_k, f, g_k belong to $L^1(0,\ell)$. Then we have a solution $a, (b_k)_k$ to the resolvent equation

$$(I + \mathbb{A})(a, (b_k)_k) \ni (f, (b_k(g_k))_k) \tag{5.3}$$

if there exist $u \in \mathrm{Dom}(A)$, $v_k \in u + \mathrm{Dom}(c_k(\cdot))$, $a = a(u)$, $b_k = b(v_k)$, and $c_k^{**} \in c_k(v_k - u)$ such that

$$a(u) + A(u) - \sum_{k=1}^K c_k^{**} \ni f \text{ and} \tag{5.4a}$$

$$b_k(v_k) + c_k^{**} = b_k(g_k),\ 1 \le k \le K,\ \text{in } L^1(0,\ell). \tag{5.4b}$$

Note that consistent choices $c_k^{**} \in c_k(v - u)$ are required for the equations in (5.4). (This part is similar to the beginning of the proof of Lemma 4.4.) The initial-boundary-value problem (5.1) takes the form of the abstract initial-value problem in $L^1(0,\ell) \times L^1(0,\ell)^K$:

$$\tfrac{d}{dt}(a(t), (b_k(t))_k) + \mathbb{A}(a(t), (b_k(t))_k) \ni (F(t), 0),\ 0 < t < T, \tag{5.5a}$$

$$(u, (v_k)_k)(0) = (u_{init}, (v_{k,init})_k). \tag{5.5b}$$

We shall apply Theorem 2.1 to obtain a C^0-solution of (5.5).

LEMMA 5.2. *The operator $\mathbb{A}$ is accretive in $L^1(0,\ell) \times L^1(0,\ell)$.*

Proof. Let $a, (b_k)_k$ and $\bar{a}, (\bar{b}_k)_k$ be solutions of the respective resolvent equations

$$(I + \mathbb{A})(a, (b_k)_k) \ni (f, (g_k)_k),\ (I + \mathbb{A})(\bar{a}, (\bar{b}_k)_k) \ni (\bar{f}, (\bar{g}_k)_k)$$

with respective representatives $u, (v_k)_k$ and $\bar{u}, (\bar{v}_k)_k$ and $\bar{a} = a(\bar{u})$, $\bar{b}_k = b_k(\bar{v}_k)$. Take differences of corresponding components and multiply the component equation differences of (5.4) by the respective selections

$$\sigma_0 = \mathrm{sgn}_0(a - \bar{a} + u - \bar{u}) \in \mathrm{sgn}(a - \bar{a}) \cap \mathrm{sgn}(u - \bar{u}),$$
$$\sigma_k = \mathrm{sgn}_0(b_k - \bar{b}_k + v_k - \bar{v}_k) \in \mathrm{sgn}(b_k - \bar{b}_k) \cap \mathrm{sgn}(v_k - \bar{v}_k).$$

Add the equations, note that $\sum (c_k^{**} - \bar{c}_k^{**})(\sigma_k - \sigma_0) \ge 0$ since each term is nonnegative a.e., and integrate to obtain

$$\|a - \bar{a}\|_{L^1} + \sum_{k=1}^K \|b_k - \bar{b}_k\|_{L^1} \le \|f - \bar{f}\|_{L^1} + \sum_{k=1}^K \|g_k - \bar{g}_k\|_{L^1}. \tag{5.6}$$

Here we have used $\int_0^\ell \big(A(u) - A(\bar{u})\big)\, \mathrm{sgn}_0(u - \bar{u})\, dx \ge 0$ since A is accretive in $L^1(0,\ell)$. This holds as well for any positive multiple of $\mathbb{A}$, so it is accretive. ∎

Lemma 5.2 shows there is at most one solution $a(t), (b_k(t))_k$. These uniquely determine $u(t)$ and $w(t)$. It remains to verify the range condition (2.4) to prove existence of a solution of the resolvent system (5.4). The equation

$$a(u) + A(u) + \sum_{k=1}^K b_k\big(u + (I + c_k)^{-1}(g_k - u)\big) = f + \sum_{k=1}^K b_k(g_k)$$

has a solution in $L^1(0,\ell)$ because the third term is monotone and Lipschitz, the first is a positive multiple of the identity plus a monotone Lipschitz function, and A is m-accretive. Then define $v_k = u + (I + c_k)^{-1}(g_k - u)$ so we have $v_k = g_k - \tilde{c}_k$, $\tilde{c}_k \in c(v_k - u)$, $1 \le k \le K$. These satisfy $b_k(v_k) = b_k(g_k) - c_k^{**}$ with $c_k^{**} \in c_k(v_k - u) \cap L^1(0,\ell)$ by Lemma 4.3, so we have a solution of the resolvent system (5.4). ∎

Copyright © by SIAM. Unauthorized reproduction of this article is prohibited.

Downloaded 05/07/20 to 128.193.164.203. Redistribution subject to SIAM license or copyright; see http://www.siam.org/journals/ojsa.php

Downloaded 05/07/20 to 128.193.164.203. Redistribution subject to SIAM license or copyright; see http://www.siam.org/journals/ojsa.php

Remark 5.3 (additional observations). (A) It is not true that $\mathbb{A}$ is m-accretive in $L^1(0,\ell) \times L^1(0,\ell)$. The range of $b_k(\cdot)$ limits the range of the second component of (5.3).

(B) By using the positive signum functions sgn^+ in place of sgn in the preceding estimates, one can obtain comparison principles. In particular, nonnegative data leads to nonnegative solutions.

(C) Finally, we note that the C^0-solution satisfies $(a(t),(b_k(t))) \in \overline{\mathrm{Dom}(\mathbb{A})}$ for $0 \le t \le T$, but it is not necessarily differentiable in either variable at any time.

6. Numerical scheme for PDE. We now discuss the numerical scheme for the homogeneous version of (5.1) posed on $\mathbb{R}$ with compactly supported initial data

$$\frac{\partial}{\partial t}\left(a(u)+w\right)+\frac{\partial}{\partial x}\alpha(u)=0,\ \ x\in\mathbb{R},\ 0<t\le T, \tag{6.1a}$$

$$w(x,t)=\mathcal{H}(u(x,t)), \tag{6.1b}$$

where $\mathcal{H}$ is defined as in (5.1b). The initial data are given by

$$u(x,0)=u_{init}(x)\,,\ v_k(x,0)=v_{k,init}(x)\,, \tag{6.1c}$$

$$u_{init}(\cdot), v_{k,init}(\cdot)\ \forall k \text{ have compact support and satisfy (5.2).}$$

Below we denote $q(u)=a(u)+w$. With this notation, (6.1) is a scalar conservation law solved for q:

$$q_t+\alpha_x=0,\ q(x,0)=q_{init}(x). \tag{6.2}$$

The flux $\alpha=(\alpha\circ u)(q)$, where $u=u(q)$ is the inverse of $q=a(u)+w$. Strictly speaking, this change of variables is only correct for smooth solutions when the chain rule applies and when $w=0$.

In section 6.1 we formulate a finite difference scheme for (6.2) and equivalently for (6.1). The scheme is upwind explicit in the transport term and resolves the nonlinearities in q implicitly with the case $w\equiv 0$ handled the same way as $w\not\equiv 0$. The analysis of the scheme differs substantially between these two cases.

If $w\equiv 0$, then $u=a^{-1}$. In this case one can eliminate u, and (6.2) is a standard problem solved for q with the flux $\alpha(q)=\alpha(a^{-1}(q))$, whose properties, such as smoothness, monotonicity, and Lipschitz continuity, are inherited from those of $a(\cdot)$ and $\alpha(\cdot)$. This case is standard; we recall the properties of an upwind numerical scheme for this case in section 6.2.

The main challenge when $w\not\equiv 0$ is addressed in section 6.3 with stability proved in an L^1-like product space. Even though the hysteresis nonlinearity is monotone, the relationship $u=u(q)$ (or, more generally, $\alpha\circ u$) is not Lipschitz due to its history dependence; this is elucidated in section 6.4. The special case of linear transport when $a=\mathrm{id}, \alpha=\mathrm{id}$ and K-linear play model, i.e., $b_k=\mu_k\mathrm{id}$, is handled in section 6.5; here we formulate L^2-like stability results in a weighted product space.

6.1. Numerical scheme for (6.2). We consider uniform spatial and time grids with parameters h,τ, respectively, and set $\nu=\frac{\tau}{h}$. We have $t_n=n\tau, n=0,1,\ldots,ow$ and $x_j=jh,\ j=-\infty,\ldots-1,0,1,\ldots\infty$. The grid norm for a grid function $G=(G_j)_{j=-\infty}^{\infty}$ is $\|\,G\,\|_{\Delta,p}=(\sum_j h\mid G_j\mid^p)^{1/p}$ with $p=1,2$. We also define $TV(G^n)=\sum_j|\,G_j^n-G_{j-1}^n\,|$, and $TV_T(G)=\sum_n \tau TV(G^n)+\|\,G^{n+1}-G^n\,\|_{\Delta,1}$. The assumption on compactly supported data makes these sums finite.

Copyright © by SIAM. Unauthorized reproduction of this article is prohibited.

Downloaded 05/07/20 to 128.193.164.203. Redistribution subject to SIAM license or copyright; see http://www.siam.org/journals/ojsa.php

Scheme. We approximate the solution to (6.2) $q(x_j, t_n) \approx Q_j^n$ with

$$Q_j^n - Q_j^{n-1} + \nu(\mathcal{A}_j^{n-1} - \mathcal{A}_{j-1}^{n-1}) = 0 \ \ \forall j. \tag{6.3a}$$

The initial values $U_j^0 = u_{init}(x_j)$ and $V_{j,k}^0 = v_{k,init}(x_j)$ satisfy (5.2).

In the process of solving (6.3) we evaluate the fluxes with explicit-in-time upwind treatment; the numerical flux denoted by $\mathcal{A}_j^{n-1} \approx \alpha(u(q))|_{x_{j+\frac{1}{2}}}$ is given by

$$\mathcal{A}_j^{n-1} = \alpha(U_j^{n-1}) \ \forall j. \tag{6.3b}$$

These require the approximations $U_j^n \approx u(x_j, t_n)$, which we find from $Q_j^n = U_j^n + W_j^n$, where $W_j^n \approx w(x_j, t_n)$. This is resolved implicitly, locally at every point x_j. While seeking W_j^n at each x_j, t_n, we also find the components $V_{k,j}^n \approx v_k(x_j, t_n)$ for $k = 1, \ldots, K$.

The scheme (6.3) is our focus with particular attention paid to the evaluation of the flux (6.3b) tied to finding $u = u(q)$, the "inverse" of $q(u) = a(u) + w$, with $\alpha(\cdot)$ applied to the result. The crux is the treatment of the hysteresis functional, implicit in this paper. The algorithm in (6.3) can be represented by the cartoon

$$Q_j^{n-1} \overset{\text{local solver}}{\longrightarrow} (U_j^{n-1}, (W_{k,j}^{n-1})_k) \overset{\text{flux evaluation}}{\longrightarrow} \mathcal{A}_j^{n-1} \overset{\text{new time step}}{\longrightarrow} Q_j^n. \tag{6.4}$$

We see the algorithm works without "setting" the primary variables.

Below we prove nonlinear stability of (6.3) under the (CFL) condition

$$0 \le \nu \max_u \tfrac{d\alpha}{du} \le 1. \tag{6.5}$$

Schemes including higher-order and, for nonimplicit treatment of hysteresis, multiple spatial dimensions can be defined, but this is outside the present scope.

Remark 6.1. For simplicity in (6.5) and in the analysis below, we refer to $\frac{d\alpha}{du}, \frac{da}{du}$ even though these are only defined a.e. It is not hard to see, however, in the analysis below that the reference to these symbols and their sign(s) can be replaced by that to the appropriate difference quotients.

6.2. Recall analysis of (6.3) when $w = 0$. Here $q = a(u)$. With (6.5) one can establish for the solution $Q = (Q^n)_n = (Q_j^n)_{j,n}$ to (6.2) the nonlinear stability

$$TV_T(Q) \le CT \tag{6.6}$$

with some constant C independent of h, τ. From this the convergence of the discrete solutions of (6.3) to the (set of) weak solutions of (6.2) is well established [31, Chapter 12].

We outline the proof of (6.6) following, e.g., [31, 30], since the two main steps will be needed in our main result. First, (i) we establish

$$TV(Q^n) \le TV(Q^{n-1}) \le \cdots \le TV(Q^0). \tag{6.7}$$

This follows by writing (6.2) at j and $j-1$, subtracting these, and applying the mean value theorem to

$$\mathcal{A}_j^{n-1} - \mathcal{A}_{j-1}^{n-1} = \chi_j(Q_j^{n-1} - Q_j^{n-1}) \tag{6.8}$$

with $\chi_j = \frac{d\alpha}{dq}|_{\xi_j} = \frac{d\alpha}{du}\frac{du}{dq}|_{\xi_j}$ and ξ_j between Q_j^{n-1}, Q_{j-1}^{n-1}. Combining terms we get

$$Q_j^n - Q_{j-1}^n = (1 - \nu\chi_j)(Q_j^{n-1} - Q_{j-1}^{n-1}) + \nu\chi_{j-1}(Q_{j-1}^{n-1} - Q_{j-2}^{n-1}).$$

Copyright © by SIAM. Unauthorized reproduction of this article is prohibited.

Downloaded 05/07/20 to 128.193.164.203. Redistribution subject to SIAM license or copyright; see http://www.siam.org/journals/ojsa.php

Taking absolute value, by triangle inequality we have

$$|Q_j^n - Q_{j-1}^n| \leq (1-\nu\chi_j)\,|Q_j^{n-1} - Q_{j-1}^{n-1}| + \nu\chi_{j-1}\,|Q_{j-1}^{n-1} - Q_{j-2}^{n-1}|,$$

where we have used that $0 \leq \nu \max_j \chi_j = \nu \max_u \frac{d\alpha}{du} \leq 1$, which follows from (6.5) and from the useful auxiliary property

$$0 \leq \tfrac{du}{dq} = \tfrac{du}{da} \leq 1 \tag{6.9}$$

implied by (2.1). Now we can sum over j and combine the sums arising on the right-hand side together since they differ by an index only. The terms multiplied by ν cancel, and we conclude the first (and each subsequent) inequality in (6.7).

Next (ii) we prove estimates on $\|Q^n - Q^{n-1}\|_{\Delta,1}$. From (6.3a), after some algebra

$$h\,|Q_j^n - Q_j^{n-1}| = \tau\,|\mathcal{A}_j^{n-1} - \mathcal{A}_{j-1}^{n-1}| \leq \tau L_\alpha\,|Q_j^{n-1} - Q_{j-1}^{n-1}|, \tag{6.10}$$

where in the estimate we have exploited the Lipschitz bound from (2.1c) on $0 \leq \frac{d\alpha}{dq} = \frac{d\alpha}{du}\frac{du}{dq} \leq \frac{d\alpha}{du} \leq L_\alpha$. Summing over j we get $\|Q^n - Q^{n-1}\|_{\Delta,1} \leq \tau L_\alpha TV(Q)$. Summing over n, with (6.7), involves $\sum_n \tau = T$, and (6.6) follows.

COROLLARY 6.2. *The results in this section apply directly to a common application to scalar adsorption problem when $a_o(\cdot)$ is a monotone nondecreasing piecewise smooth adsorption isotherm. In particular, we infer convergence of (vanishing viscosity solutions satisfying the entropy condition to) the scheme* (6.3) *to the space of weak solutions to* (6.2)*, with the rate of at most $O(h)$ for smooth solutions and $O(\sqrt{h})$ for problems involving shocks.*

6.3. Scheme for adsorption hysteresis. Now we consider (6.1), in which $w = \mathcal{H}(u)$, which is the main challenge. At every time step t_n, $n = 1, 2, \ldots$, and at every j, we follow the outline (6.4) for (6.3). We rewrite (6.3) in terms of primary variables to emphasize the elements needed in subsequent analysis.

Given $(U_j^{n-1})_j, ((V_{k,j}^{n-1})_k)_j$, (or Q_j^{n-1}) at every j, we solve for the new time step values $U_j^n, (V_{k,j}^n)_k, W_j^n$, which satisfy

$$a(U_j^n) - a(U_j^{n-1}) + W_j^n - W_j^{n-1} = -\nu(\mathcal{A}_j^{n-1} - \mathcal{A}_{j-1}^{n-1}), \tag{6.11a}$$

$$W_j^n = \sum_k b_k(V_{k,j}^n), \quad V_{k,j}^n = U_j^n + R_k(V_{k,j}^{n-1} - U_j^n) \ \ \forall k. \tag{6.11b}$$

Note that while $V_{k,j}^n$ is given explicitly in (6.11b) in terms of resolvent R_k, its value depends on U_j^n; thus, (6.11b) is coupled nonlinearly to (6.11a), which in turn uses W_j^n defined in (6.11b). The solvability of this coupling follows from Proposition 4.5 since (6.11) is analogous to (4.5) with the input τf^n in (4.5a) analogous to $f_j^n = -\nu(\mathcal{A}_j^{n-1} - \mathcal{A}_{j-1}^{n-1})$ in (6.11a).

Our main result is the stability of the scheme (6.11) or, equivalently, of (6.3). The results are formulated in the product space $L^1 \times (L^1)^K$ with the l^1 norm on the product used for shorthand $\|(u, (w_k)_k)\| = \|u\| + \sum_k \|w_k\|$. (We also work in weighted l_2 norms on the product in section 6.5.) We denote $U = (U_j^n)_{j,n}$ and $a(U)$ denotes $a(U_j^n)_{j,n}$. We denote $W_{j,k}^n = b_k(V_{k,j}^n)$, $W_k^n = ((W_{k,j}^n)_{j,n})_j$, $W_k = (W_k^n)^n$ and consider

Copyright © by SIAM. Unauthorized reproduction of this article is prohibited.

Downloaded 05/07/20 to 128.193.164.203. Redistribution subject to SIAM license or copyright; see http://www.siam.org/journals/ojsa.php

$(W_k)_k$. We also define

$$\begin{aligned} TV(a(U^n)) &= \sum_j |\, a(U_j^n) - a(U_{j-1}^n)\,|, \\ TV((W_k^n)_k) &= \sum_{k,j} |\, W_j^n - W_{j-1}^n\,|, \\ TV_T(a(U),(W_k)_k) &= \sum_n \tau \left(TV(a(U^n)) + \sum_k TV((W_k^n)_k) \right) \\ &\quad + \|\, a(U^{n+1}) - a(U^n)\,\|_{\Delta,1} + \sum_n \sum_k \|\, W_k^{n+1} - W_k^n\,\|_{\Delta,1}. \end{aligned}$$

The notation simplifies if $a = \mathrm{id}$.

Our goal is to show

$$TV_T(a(U),(W_k)_k) \le C(T). \tag{6.12}$$

We prove (6.12) in two stages. In section 6.3.1 we first deal with the case $a = \mathrm{id}$, $\alpha = \mathrm{id}$, and in section 6.3.2 formulate the general result on stability. Our approach to stability in the product space is different than that for nonhysteresis case and scalar unknown $Q = (Q_j^n)_{j,n}$ in section 6.2. The latter relies on differentiability of (and the Lipschitz bounds for) the flux function $\alpha = \alpha(q)$; see, e.g., (6.8) and (6.10), where these properties are exploited. As we mentioned these properties do not carry over to the hysteresis case; see section 6.4 for details.

6.3.1. Nonlinear stability for the case $a = \mathrm{id}$, $\alpha = \mathrm{id}$.

THEOREM 6.3. *Assume* $a = \mathrm{id}$, $\alpha = \mathrm{id}$, (2.1b) *and* (6.1c), *and that the CFL condition* (6.5) *holds. Then the solution* $(U,(W_k)_k)$ *to* (6.11) *is* (i) *stable and* (ii) *TV-stable on the product space* $L^1 \times (L^1)^K$*; i.e.,* (6.12) *holds.*

Proof. To prove the results, we follow the steps in section 6.2 which we combine with the estimates in section 4.3.

Stability. We first consider $\sum_j |\, U_j^n\,| + \sum_{k,j} |\, W_{k,j}^n\,|$. We rewrite (6.11) with $a = \mathrm{id}, \alpha = \mathrm{id}$, and we revert from the resolvent formulation with R_k back to that with the selection c_k^*; see Remark 4.1. At every j the tuple $(U_j^n,(W_{k,j}^n)_k)$ satisfies $W_{k,j}^n = b_k(V_{k,j}^n)$:

$$U_j^n + \sum_k b_k(V_{k,j}^n) = (1-\nu)U_j^{n-1} + \nu U_{j-1}^{n-1} + \sum_k b_k(V_{k,j}^{n-1}), \tag{6.13a}$$

$$V_{k,j}^n + c_{k,j}^* = V_{k,j}^{n-1},\ c_{k,j}^* \in c_k(V_{k,j}^n - U_j^n)\ \forall k. \tag{6.13b}$$

This local nonlinear problem (6.13) solved for $U_j^n,(W_{k,j}^n)_k$ has the same structure as (4.6a) in Lemma 4.4 with $f = (1-\nu)U_j^{n-1} + \nu U_{j-1}^{n-1}$ and $g_k = V_{k,j}^{n-1}$. By (4.8) we obtain, also applying (6.5), from which we have $0 \le \nu \le 1$,

$$|\, U_j^n\,| + \sum_k |\, b_k(V_{k,j}^n)\,| \le (1-\nu)\,|\, U_j^{n-1}\,| + \nu\,|\, U_{j-1}^{n-1}\,| + \sum_k |\, b_k(V_{k,j}^{n-1})\,|\,.$$

After we sum both sides over j, we combine together the two sums involving U_j^{n-1}

Copyright © by SIAM. Unauthorized reproduction of this article is prohibited.

and U_{j-1}^{n-1} which differ by an index to get $\sum_j |U_j^{n-1}|$. Multiply by h to get

$$\begin{aligned}\|(U^n,(W_k^n)_k\|_{\Delta,1} &= h\sum_j |U_j^n| + h\sum_{j,k} |b_k(V_{k,j}^n)| \\ &\le h\sum_j |U_j^{n-1}| + h\sum_{j,k} |b_k(V_{k,j}^{n-1})| = \|(U^{n-1},(W_k^{n-1})_k\|_{\Delta,1}.\end{aligned}$$

Applying the last estimate recursively for $n-1, n-2, \dots$ we find (i) is proven.

TV-stability. The estimates for TV are done similarly. We rewrite the system (6.13) for $j-1$, subtract it from that for j, and apply the comparison part (4.7) of Lemma 4.4, and upon (6.5) we find

$$\begin{aligned}|U_j^n - U_{j-1}^n| + \sum_k |b_k(V_{k,j}^n) - b_k(V_{k,j-1}^n)| \le |U_j^{n-1} - U_{j-1}^{n-1}|\,(1-\nu) + \nu\,|U_{j-1}^{n-1} - U_{j-2}^{n-1})| \\ + \sum_k |b_k(V_{k,j}^{n-1}) - b_k(V_{k,j-1}^{n-1})|\,.\end{aligned}$$

Summing over j and collapsing the first and second sums together on the right-hand side yields

$$TV(U^n) + \sum_k TV(W_k^n) \le TV(U^{n-1}) + \sum_k TV(W_k^{n-1}),$$

and applying recursively this yields

$$TV(U^n) + \sum_k TV(W_k^n) \le \cdots \le TV(U^0) + \sum_k TV(W_k^0). \tag{6.14}$$

Variation in time. Finally, we prove that the variation in time is bounded. This requires a finer control on each of $U_j^n - U_j^{n-1}$ and $W_j^n - W_j^{n-1}$ than that on $Q_j^n - Q_j^{n-1}$ seen in (6.10). This additional information comes from Proposition 4.6 applied to (6.11) to yield

$$|U_j^n - U_j^{n-1}| + \sum_k |W_{k,j}^n - W_{k,j}^{n-1}| = \nu\,|U_j^{n-1} - U_{j-1}^{n-1}|\,. \tag{6.15}$$

Multiplying both sides by h and summing over j we get

$$\|U^n - U^{n-1}\|_{\Delta,1} + \sum_k \|W_k^n - W_k^{n-1}\|_{\Delta,1} = \tau TV(U^{n-1}).$$

Summing over n and combining with (6.14) we obtain

$$\begin{aligned}TV_T(U,(W_k)_k) &= \sum_n \tau TV(U^n,(W_k^n)_k) \\ &\quad + \sum_n \left(\|U^n - U^{n-1}\|_{\Delta,1} + \sum_k \|W_k^n - W_k^{n-1}\|_{\Delta,1}\right) \le T(C^0+1),\end{aligned}$$

where C^0 is the constant on the right-hand side of (6.14). This completes the proof. ∎

Copyright © by SIAM. Unauthorized reproduction of this article is prohibited.

Downloaded 05/07/20 to 128.193.164.203. Redistribution subject to SIAM license or copyright; see http://www.siam.org/journals/ojsa.php

Downloaded 05/07/20 to 128.193.164.203. Redistribution subject to SIAM license or copyright; see http://www.siam.org/journals/ojsa.php

6.3.2. The case $a \neq$ id, $\alpha \neq$ id. The extension of Theorem 6.3 to the case $a \neq$ id deserves a few notes. We write the analogue of (6.13a) written with $a(U_j^n)$ replacing U_j^n:

$$a(U_j^n) + \sum_k b_k(V_{k,j}^n) = a(U_j^{n-1}) - \nu \mathcal{A}_j^{n-1} + \nu \mathcal{A}_{j-1}^{n-1} + \sum_k b_k(V_{k,j}^{n-1}), \tag{6.16a}$$

$$V_{k,j}^n + c_{k,j}^* = V_{k,j}^{n-1},\ c_{k,j}^* \in c_k(V_{k,j}^n - U_j^n)\ \forall k. \tag{6.16b}$$

First we demonstrate TV-stability in some detail; stability follows with very similar calculations. We subtract (6.16) for j and $j-1$ and apply the comparison part of Lemma 4.4 to get

$$\begin{aligned} |a(U_j^n) - a(U_{j-1}^n)| + \sum_k |b_k(V_{k,j}^n) - b_k(V_{k,j-1}^n)| \\ \leq |a(U_j^{n-1}) - a(U_{j-1}^{n-1}) - \nu(\mathcal{A}_j^{n-1} - \mathcal{A}_{j-1}^{n-1}) + \nu(\mathcal{A}_{j-1}^{n-1} - \mathcal{A}_{j-2}^{n-1})| \\ + \sum_k |b_k(V_{k,j}^{n-1}) - b_k(V_{k,j-1}^{n-1})|\,. \end{aligned}$$

Next we use the strong monotonicity of $a(\cdot)$ to write

$$a(U_j^{n-1}) - a(U_{j-1}^{n-1}) = \sigma_a(U_j^{n-1} - U_{j-1}^{n-1})$$

with some σ_a, different at each point in which it is applied. Now by (2.1a), $\sigma_a \geq 1$. Further, continuing with the first term on the right-hand side we use $\gamma_j = \frac{d\alpha}{du}|_{\delta_j}$ with δ_j between U_j^{n-1} and U_{j-1}^{n-1}. Proceeding similarly as in section 6.2 we get

$$\begin{aligned} &|a(U_j^{n-1}) - a(U_{j-1}^{n-1}) - \nu(\mathcal{A}_j^{n-1} - \mathcal{A}_{j-1}^{n-1}) + \nu(\mathcal{A}_{j-1}^{n-1} - \mathcal{A}_{j-2}^{n-1})| \\ &\quad = |\sigma_a(U_j^{n-1} - U_{j-1}^{n-1}) - \nu\gamma_j(U_j^{n-1} - U_{j-1}^{n-1}) + \nu\gamma_{j-1}(U_{j-1}^{n-1} - U_{j-2}^{n-1})| \\ &\qquad \leq (\sigma_a - \nu\gamma_j)\,|U_j^{n-1} - U_{j-1}^{n-1}| + \nu\gamma_{j-1}\,|U_{j-1}^{n-1} - U_{j-2}^{n-1}| \end{aligned}$$

noticing $\sigma_a - \nu\gamma_j \geq 0$ by (6.5). Next we follow the same calculations as those leading to (6.14), summing over j and eliminating the sums with factors γ_j and γ_{j-1}. After that, we can go back to the variables $a(U_j^{n-1}) - a(U_{j-1}^{n-1})$. Thus, we obtain

$$\sum_j |a(U_j^n) - a(U_{j-1}^n)| + \sum_k TV(W_k^n) \leq \sum_j |a(U_j^{n-1}) - a(U_{j-1}^{n-1})| + \sum_k TV(W_k^{n-1}).$$

Applying this estimate recursively we can bound the quantity on the left-hand side at time step n by that at t_0, which we call $C^{a,0}$. Due to coercivity of $a(\cdot)$ and $|U_j^n - U_j^n| \leq |a(U_j^n) - a(U_{j-1}^n)|$ we can also obtain

$$\sum_j |U_j^n - U_{j-1}^n| + \sum_k TV(W_k^n) \leq C^{a,0}. \tag{6.17}$$

Finally, the statement on $TV_T(a(U), (W_k)_k)$ can be derived as follows. We start with (6.15) applied to (6.13) given in Proposition 4.5:

$$|a(U_j^n) - a(U_j^{n-1})| + \sum_k |W_{k,j}^n - W_{k,j}^{n-1}| = \nu\,|\mathcal{A}_j^{n-1} - \mathcal{A}_{j-1}^{n-1}|\,. \tag{6.18}$$

Copyright © by SIAM. Unauthorized reproduction of this article is prohibited.

Downloaded 05/07/20 to 128.193.164.203. Redistribution subject to SIAM license or copyright; see http://www.siam.org/journals/ojsa.php

Now we sum over j. The right-hand side can be bounded if we apply Lipschitz property of α along with (6.17) so that (the sum of) the right-hand side by $\sum_j \nu \mid \mathcal{A}_j^{n-1} - \mathcal{A}_{j-1}^{n-1} \mid \leq \nu C_\alpha C^{a,0}$. A few more steps collecting the results yield finally our result.

THEOREM 6.4. *Assume* (2.1a)–(2.1c) *and* (6.1c). *Then* (6.12) *holds.*

6.4. Why the estimates in section 6.2 do not work for $Q = U + W$. Now we explain why the approach in section 6.2 cannot be extended to cover the hysteresis model and why the estimates in Q^n variables do not work for the hysteresis case.

The crucial steps in the stability proof in section 6.2 are (6.8) and (6.10), in which the dependence of u on q and of α on q are exploited in the statements involving "secants," such as the estimates on $U_j - U_{j-1}$ involving $Q_j - Q_{j-1}$ or of $\mathcal{A}_j - \mathcal{A}_{j-1}$ involving $Q_j - Q_{j-1}$. We have here for $a = id + a_0$ that

$$Q_j^n = U_j^n + a_0(U_j^n) \tag{6.19}$$

so that $U_j^n - U_{j-1}^n = \frac{1}{1+\gamma_j}(Q_j^n - Q_{j-1}^n)$ with an appropriately chosen $\gamma_j \geq 0$.

However, in the hysteresis case this is not doable. To see why, consider the simplest case $K = 1, a = \mathrm{id}, b = \mathrm{id}, \alpha = \mathrm{id}$. We have

$$Q_j^n = U_j^n + W_j^n, \;\; W_j^n = U_j^n + R(W_j^{n-1} - U_j^n) \tag{6.20}$$

(see, e.g, (6.11b)). The dependence of U_j^n, Q_j^n on the history via W_j^{n-1} cannot be eliminated. While the flux $\mathcal{A}_j^n$ defined by (6.3b) is Lipschitz in the variable U_j^n, its dependence on the primary known Q_j^n involves also the dependence on W_j^{n-1}. The latter dependence, while also Lipschitz, requires keeping track of the history of the evolution, as the hysteresis operator requires. Estimating directly the variable Q_j^n would require keeping track of telescoping sums over the history of time steps and would not yield stability in the usual sense. This last conjecture is based on our experience reported for a related but linear case in [36].

Nevertheless, our main result formulated in the product space in Theorem 6.4 and proven with monotonicity techniques holds.

6.5. L^2 stability for K-linear play model and linear transport with $a = \mathrm{id}, \alpha = \mathrm{id}$. In this case we obtain a more refined result in weighted Hilbert space setting, exploiting an idea from [36] defined for linear functions $c(\cdot)$ rather than graphs. Consider (6.13) again. We have $b_k = \mu_k \mathrm{id}$; thus,

$$U_j^n - \sum_k \mu_k c_k^* = (1-\nu)U_j^{n-1} + \nu U_{j-1}^{n-1}, \tag{6.21a}$$

$$V_{k,j}^n + c_k^* = V_{k,j}^{n-1}, \; c_k^* \in c_k(V_{k,j}^n - U_j^n) \; \forall k. \tag{6.21b}$$

We multiply (6.21a) by U_j^n and (6.21b) by $\mu_k V_{k,j}^n$ and add both equations to get

$$\begin{aligned}(U_j^n)^2 + \sum_k \mu_k (V_{k,j}^n - U_j^n) c_k^* + \sum_k \mu_k (V_{k,j}^n)^2 \\ = (1-\nu)U_j^{n-1}U_j^n + \nu U_{j-1}^{n-1}U_j^n + \sum_k V_{k,j}^{n-1} V_{k,j}^n.\end{aligned}$$

Now the second term on the left-hand side is nonnegative because each of its summands is. On the right-hand side we apply Cauchy–Schwarz inequality componentwise

Copyright © by SIAM. Unauthorized reproduction of this article is prohibited.

Downloaded 05/07/20 to 128.193.164.203. Redistribution subject to SIAM license or copyright; see http://www.siam.org/journals/ojsa.php

and rearrange

$$(U_j^n)^2 + \sum_k \mu_k (V_{k,j}^n)^2 \le \frac{1}{2}\left((1-\nu)\left((U_j^{n-1})^2 + (U_j^n)^2\right) + \nu\left((U_j^n)^2 + (U_{j-1}^{n-1})^2\right)\right) + \frac{1}{2}\sum_k \mu_k \left((V_{k,j}^{n-1})^2 + (V_{k,j}^n)^2\right).$$

Now we add up the right-hand-side terms corresponding to the step n, kick these back to the left-hand side, and eliminate the factor $\frac{1}{2}$ from both sides. After we sum over j, the sums involving $(1-\nu)\sum_j (U_j^{n-1})^2$ and $\nu \sum_j (U_{j-1}^{n-1})^2$ can be combined together to yield $\sum_j (U_j^{n-1})^2$. Thus, we obtain

$$\sum_j (U_j^n)^2 + \sum_j \sum_k \mu_k (V_{k,j}^n)^2 \le \sum_j (U_j^{n-1})^2 + \sum_j \sum_k \mu_k (V_{k,j}^{n-1})^2.$$

Multiplication of both sides by h gives the desired stability result of

$$\| (U^n, (V_k^n)_k) \|_{\Delta,\mu} \le \| (U^{n-1}, (V_k^{n-1})_k) \|_{\Delta,\mu} \tag{6.22}$$

in the grid norm $\|\cdot\|_{\Delta,\mu}$ on the $(1, (\sqrt{\mu_k})_k)$ weighted space $(L^2)^{K+1}$.

Remark 6.5. The stability results obtained here suggest that there should be convergence in L^2 norm for the K-linear play model. For sufficiently smooth solutions we expect even $O(h)$ rate.

7. Numerical results. In this section we briefly report on numerical experiments on the convergence of the scheme 6.3. We choose $\alpha = \mathrm{id}, a = \mathrm{id}$; more extensive results including those with $a \neq \mathrm{id}, \alpha \neq \mathrm{id}$ will be reported elsewhere. A particular aspect worth special mention is the piecewise linear character of the scanning curves defining the graph and the related piecewise behavior of the rarefaction waves.

The stability results in Theorem 6.4 and Corollary 6.5 are formulated for the tuple $(u, (w_k)_k)$. However, with large K it is more practical to estimate the error in $w = \sum_k w_k$. Below we use notation $e_u = u - U$, $e_w = w - W$, and $\| e \|_{\Delta,p}$ defined on the product space for $p = 1$, $p = 2$ as in section 7. The number α_p is an estimated order of $\| e \|_{\Delta,p}$.

Regarding convergence, since our scheme is not fully implicit as (2.6), the theory reported in [46] does not strictly apply, even if we pursue the method-of-lines approach. However, one can conjecture that the convergence of the semidiscrete part of (6.3) should be about $O(\tau)$ in Hilbert space when the operator is a subgradient, $O(\sqrt{\tau})$ in Banach space with an m-accretive operator, or one satisfying the range condition as in Theorem 5.1. Considering the contribution of the error in spatial discretization (at best $O(h)$), upon CFL condition (6.5), this yields $O(\sqrt{h})$ for K-nonlinear play and at best $O(\sqrt{h})$ even for the case of smooth solutions with K-linear play $\mathcal{H}(u)$ since the spatial transport operator is not a subgradient.

However, below we demonstrate $O(\sqrt{h})$ convergence for the K-nonlinear play model (1.1) and close to $O(h)$ rate for the K-linear play hysteresis case (1.2) both in the L^1 and in the L^2 setting. Strictly speaking, the latter results seem to be of superconvergence due to smoothness shown in [44] of solutions to transport models with convex-concave $\mathcal{H}$; these are continuous, with only a few points of nondifferentiability. It is also possible that the numerical diffusion is associated with the upwind scheme.

Finally, we remark that the scheme (6.3) is quite robust. We use a range of h with $\nu = 1$. The local nonlinear solver works well; we set absolute tolerance to 10^{-14}

Copyright © by SIAM. Unauthorized reproduction of this article is prohibited.

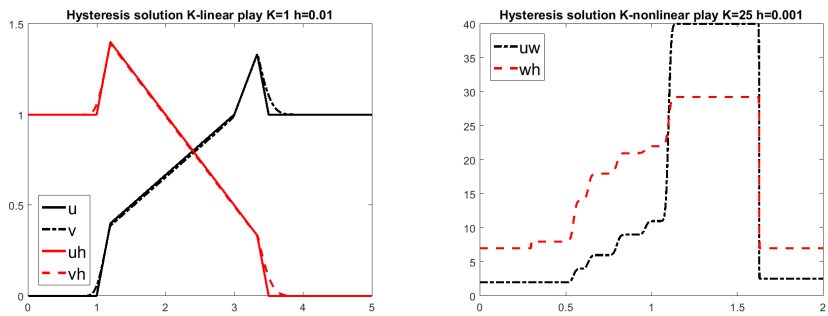

FIG. 4. *Left: exact and numerical solution for linear play model at $T = 8$. Right: numerical solution for K-nonlinear play model at $T = 1$.*

TABLE 1
Convergence for linear play model. We use the exact solution from [44] *as well as that estimated from fine grid solution $h = 0.001$.*

h	$\|e\|_{\Delta,1}$	α_1	$\|\bar{e}\|_{\Delta,1}$	$\bar{\alpha}_1$	$\|e\|_{\Delta,2}$	α_2	$\|\bar{e}\|_{\Delta,2}$	$\bar{\alpha}_2$
0.1	0.6079		0.5941		0.4341		0.2782	
0.05	0.3452	0.8163	0.3355	0.8243	0.2463	0.8173	0.1703	0.7079
0.01	0.08167	0.8718	0.07309	0.9101	0.05809	0.8735	0.04528	0.7885
0.005	0.04205	0.8917	0.03353	0.9596	0.02987	0.8934	0.02284	0.8344
0.001	0.00849	0.9272			0.006036	0.9284		

and relative tolerance to 10^{-6}. The solver never needs more than 3 (5 in K-nonlinear play case) and on average 1.11 iterations (fewer than 1 in K-nonlinear play case).

7.1. Hysteresis linear play model with $\alpha = -1, \beta = 1$. Here we follow [44], where an analytical solution is given. The graph $\mathcal{H}$ is the linear play model shown in Figure 2, left. The initial data is a piecewise "hat" function u_{init} prescribed on $(0, 5)$ and supplemented with boundary data for $0 \le t \le T = 8$. The solution $u(t), v(t)$ remains continuous and develops rarefactions in the front and back of the wave due to the convex-concave character of the flux function shown in Figure 1, right.

The numerical solution for $h = 0.01$ shown against exact solution in Figure 4 shows some numerical diffusion concentrated near corners of the solution; nevertheless, it converges with rate close to linear in $\|\cdot\|_{\Delta,1}$ as shown in Table 1. When testing against a fine grid solution ($h = 0.001$) instead of the exact solution, we report on the estimates $\|\bar{e}\|_{\Delta,1}$ and $\bar{\alpha}_1$ instead of $\|e\|_{\Delta,1}$ and α_1. The linear rate is confirmed. In addition, the convergence rate in the Hilbert space case $\|e\|_{\Delta,2}$ norm is similar to that in $\|e\|_{\Delta,1}$.

The perfectly linear convergence rate can be obtained if we rig a case in which $u(x,t)$ and $v(x,t)$ are smooth and develop as few "corners" as possible. This is possible, e.g., if we set $u_{init}(x) = 2 - \sin(\frac{\pi x}{10})$ and $v_{init}(x) = u_{init}(x) - 1$. Over $0 \le t \le T = 1$ the solutions $u(x,t) = u_{init}(x - \frac{t}{2})$ and $v(x,t) = u(x,t) - 1$, and the convergence rate is indeed $O(h)$, as shown in Table 2. Of course, this special case reduces simply to a linear transport model. More generally, to obtain a smooth solution for the hysteresis linear play case we can ensure that the portions of the $\mathcal{H}(u)$ graph traveled during the evolution exhibit very few corners, which happens when the paths of the flux function are effectively piecewise linear with few switches.

Clearly, the solution is substantially less smooth for the K-nonlinear play model discussed below.

Copyright © by SIAM. Unauthorized reproduction of this article is prohibited.

Downloaded 05/07/20 to 128.193.164.203. Redistribution subject to SIAM license or copyright; see http://www.siam.org/journals/ojsa.php

Downloaded 05/07/20 to 128.193.164.203. Redistribution subject to SIAM license or copyright; see http://www.siam.org/journals/ojsa.php

TABLE 2
Convergence with linear play model and simple traveling wave solution.

h	$\|e\|_{\Delta,1}$	α_1	$\|e\|_{\Delta,2}$	α_2
0.1	0.006769		0.004786	
0.05	0.003356	1.012	0.002373	1.012
0.01	0.0006669	1.006	0.0004715	1.006
0.005	0.0003332	1.005	0.0002356	1.005
0.001	6.659e-05	1.004	4.708e-05	1.004

TABLE 3
Convergence with K-nonlinear play hysteresis model $K = 25$.

h	$\|\bar{e}\|_{\Delta,1}$	$\bar{\alpha}_1$
0.1	7.423	
0.05	4.996	0.5712
0.01	1.705	0.6389
0.005	0.9158	0.6985

7.2. K-nonlinear play hysteresis example. Here we demonstrate the properties of solutions with the hysteresis graph from section 3.2 with $K = 25$ auxiliary functions $v_k(t)$. We set up $x \in [0, 2]$ and initial condition to be a "box" $u_{init}(x) = 40$ when $0.3 < x < 1$ and 2 otherwise. We run the simulation until $T = 1$.

The hysteresis graph is concave-concave; thus, the flux function is convex-convex; see Figure 1, right. The solution U maintains therefore a shock in front, followed by a stepwise rarefaction wave. The piecewise behavior of the rarefaction develops due to the piecewise linear envelope of the "down" scanning curve of the hysteresis functional.

We do not have exact solution; thus, in Table 3 we present convergence rate estimated from fine grid solution (with $h = 0.001$). The rate appears close to $O(\sqrt{h})$, as expected.

8. Conclusions and extensions. In this paper we formulated a new practical K-nonlinear play hysteresis model (1.1) applicable to transport with adsorption. With a slew of auxiliary results we proved well-posedness of the PDE model as well as the nonlinear stability of a robust explicit-implicit scheme (6.3) which appears to converge with the rate $O(\sqrt{h})$ similar to that for usual scalar conservation laws with increasing flux functions. In some cases when the solutions are smooth and the history of the evolution does not involve too many switchbacks, the convergence appears to be $O(h)$, also in L^2; this is similar to the case of nearly linear flux functions.

Our results are new even though they share similarities with the well-established results on upwind schemes [30] as well as with those for fully implicit schemes (2.6) for m-accretive operators [46]. Strictly speaking, the latter would only apply via method of lines; moreover, fully implicit schemes for transport are known to be quite diffusive and therefore impractical; finally, the operator for (1.1) is not m-accretive. In turn, we cannot follow the former because the Lipschitz properties of the flux function do not hold due to the history dependence of the nonlinear operator. Nevertheless, we analyze the scheme in a product space, and the convergence rate in numerical experiments is consistent with that which hold for these general frameworks.

Many open questions remain, and some work is under way. In the companion paper [43] we consider the approximation properties of the hysteresis functional, i.e., of the (u, w) relationship. Other topics, such as schemes other than implicit in time, higher-order schemes, and those for $\mathbb{R}^d$, $d > 1$, are subjects of current work. Finally,

Copyright © by SIAM. Unauthorized reproduction of this article is prohibited.

this paper only addresses one component. The next big challenge would be to account for a coupled system of multicomponent adsorption with hysteresis such as in [50, 45].

Acknowledgments. The authors would like to thank the reviewers and editors for their suggestions that helped to improve the paper.

REFERENCES

[1] B. Albers, *Modeling the hysteretic behavior of the capillary pressure in partially saturated porous media: A review*, Acta Mech., 225 (2014), pp. 2163–2189, https://doi.org/10.1007/s00707-014-1122-4.

[2] B. Albers and P. Krejčí, *Unsaturated porous media flow with thermomechanical interaction*, Math. Methods Appl. Sci., 39 (2016), pp. 2220–2238, https://doi.org/10.1002/mma.3635.

[3] V. Barbu, *Nonlinear Semigroups and Differential Equations in Banach Spaces*, Editura Academiei Republicii Socialiste România, Bucharest, 1976, translated from the Romanian.

[4] J. W. Barrett, H. Kappmeier, and P. Knabner, *Lagrange-Galerkin approximation for advection-dominated contaminant transport with nonlinear equilibrium or non-equilibrium adsorption*, in Modeling and Computation in Environmental Sciences (Stuttgart, 1995), Notes Numer. Fluid Mech. 59, Vieweg, Braunschweig, Germany, 1997, pp. 36–48.

[5] J. W. Barrett and P. Knabner, *Finite element approximation of the transport of reactive solutes in porous media.* I. *Error estimates for nonequilibrium adsorption processes*, SIAM J. Numer. Anal., 34 (1997), pp. 201–227, https://doi.org/10.1137/S0036142993249024.

[6] J. W. Barrett and P. Knabner, *Finite element approximation of the transport of reactive solutes in porous media.* II. *Error estimates for equilibrium adsorption processes*, SIAM J. Numer. Anal., 34 (1997), pp. 455–479, https://doi.org/10.1137/S0036142993258191.

[7] J. W. Barrett and P. Knabner, *An improved error bound for a Lagrange-Galerkin method for contaminant transport with non-Lipschitzian adsorption kinetics*, SIAM J. Numer. Anal., 35 (1998), pp. 1862–1882, https://doi.org/10.1137/S0036142996301512.

[8] S. Bartels, *Quasi-optimal error estimates for implicit discretizations of rate-independent evolutions*, SIAM J. Numer. Anal., 52 (2014), pp. 708–716, https://doi.org/10.1137/130933964.

[9] F. Bassetti, *Variable time-step discretization of degenerate evolution equations in Banach spaces*, Numer. Funct. Anal. Optim., 24 (2003), pp. 391–426, https://doi.org/10.1081/NFA-120022930.

[10] P. Bénilan, *Équations d'évolution dans un espace de Banach quelconque et applications*, Univ. Paris, Orsay, 1972.

[11] P. Bénilan, *Solutions intégrales d'équations d'évolution dans un espace de Banach*, C. R. Acad. Sci. Paris Sér. A-B, 274 (1972), pp. A47–A50.

[12] A. Bermúdez, D. Gómez, and P. Venegas, *Mathematical analysis and numerical solution of models with dynamic Preisach hysteresis*, J. Comput. Appl. Math., 367 (2020), 112452, 18, https://doi.org/10.1016/j.cam.2019.112452.

[13] H. Brézis, *Opérateurs maximaux monotones et semi-groupes de contractions dans les espaces de Hilbert*, North-Holland Math. Stud. 5, North-Holland, Amsterdam, 1973, Notas de Matemática (50).

[14] M. Brokate and J. Sprekels, *Hysteresis and Phase Transitions*, Appl. Math. Sci. 121, Springer-Verlag, New York, 1996, https://doi.org/10.1007/978-1-4612-4048-8.

[15] C. Burgess, D. H. Everett, and S. Nuttall, *Adsorption hysteresis in porous materials*, Pure Appl. Chem., 61 (1989), pp. 1845–1852.

[16] M. G. Crandall, *The semigroup approach to first order quasilinear equations in several space variables*, Israel J. Math., 12 (1972), pp. 108–132, https://doi.org/10.1007/BF02764657.

[17] M. G. Crandall and L. C. Evans, *On the relation of the operator $\partial/\partial s + \partial/\partial\tau$ to evolution governed by accretive operators*, Israel J. Math., 21 (1975), pp. 261–278.

[18] M. G. Crandall and T. M. Liggett, *Generation of semi-groups of nonlinear transformations on general Banach spaces*, Amer. J. Math., 93 (1971), pp. 265–298, https://doi.org/10.2307/2373376.

[19] B. Detmann, P. Krejčí, and E. Rocca, *Solvability of an unsaturated porous media flow problem with thermomechanical interaction*, SIAM J. Math. Anal., 48 (2016), pp. 4175–4201, https://doi.org/10.1137/16M1056365.

[20] V. M. Devigne, I. S. Pop, C. J. van Duijn, and T. Clopeau, *A numerical scheme for the pore-scale simulation of crystal dissolution and precipitation in porous media*, SIAM J. Numer. Anal., 46 (2008), pp. 895–919, https://doi.org/10.1137/060673485.

Downloaded 05/07/20 to 128.193.164.203. Redistribution subject to SIAM license or copyright; see http://www.siam.org/journals/ojsa.php

Copyright © by SIAM. Unauthorized reproduction of this article is prohibited.

[21] E. El Behi-Gornostaeva, K. Mitra, and B. Schweizer, *Traveling wave solutions for the Richards equation with hysteresis*, IMA J. Appl. Math., 84 (2019), pp. 797–812, https://doi.org/10.1093/imamat/hxz015.

[22] L. C. Evans, *Application of Nonlinear Semigroup Theory to Certain Partial Differential Equations*, in Nonlinear Evolution Equations (Proc. Sympos., Univ. Wisconsin, Madison, WI, 1977), Publ. Math. Res. Center Univ. Wisconsin 40, Academic Press, New York, 1978, pp. 163–188.

[23] D. Flynn, J. P. O'Kane, and A. Zhezherun, *Numerical solution of ODEs involving the derivative of a Preisach operator and with discontinuous RHS*, J. Phys. Conf. Ser., 55 (2006), pp. 63–73, https://doi.org/10.1088/1742-6596/55/1/006.

[24] E. Godlewski and P.-A. Raviart, *Numerical Approximation of Hyperbolic Systems of Conservation Laws*, Vol. 118, Springer, New York, 2013.

[25] A. T. Kan, G. Fu, and M. B. Tomson, *Adsorption/desorption hysteresis in organic pollutant and soil/sediment interaction*, Environ. Sci. Technol., 28 (1994), pp. 859–867.

[26] E. Kierlik, P. A. Monson, M. L. Rosinberg, L. Sarkisov, and G. Tarjus, *Capillary condensation in disordered porous materials: Hysteresis versus equilibrium behavior*, Phys. Rev. Lett., 87 (2001), 055701, https://doi.org/10.1103/PhysRevLett.87.055701.

[27] P. Kordulova, *Quasilinear hyperbolic equations with hysteresis*, Journal of Physics: Conference Series, 55 (2006), pp. 135–143; International Workshop on Multi-Rate Processes and Hysteresis.

[28] C. Kossack et al., *Comparison of reservoir simulation hysteresis options*, in SPE Annual Technical Conference and Exhibition, Society of Petroleum Engineers, Richardson, TX, 2000, https://doi.org/10.2118/63147-MS.

[29] M. A. Krasnoselskii and A. V. Pokrovskiĭ, *Systems with Hysteresis*, Springer-Verlag, Berlin, 1989, https://doi.org/10.1007/978-3-642-61302-9.

[30] R. J. LeVeque, *Numerical Methods for Conservation Laws*, 2nd ed., Lectures in Mathematics ETH Zürich, Birkhäuser Verlag, Basel, 1992, https://doi.org/10.1007/978-3-0348-8629-1.

[31] R. J. LeVeque, *Finite Volume Methods for Hyperbolic Problems*, Cambridge Texts Appl. Math., Cambridge University Press, Cambridge, 2002, https://doi.org/10.1017/CBO9780511791253.

[32] T. D. Little and R. E. Showalter, *Semilinear parabolic equations with Preisach hysteresis*, Differential Integral Equations, 7 (1994), pp. 1021–1040.

[33] I. D. Mayergoyz, *Mathematical Models of Hysteresis*, Springer-Verlag, New York, 1991.

[34] M. D. Donohue and L. Aranovich, *Adsorption hysteresis in porous solids*, J. Colloid Interface Sci., 205 (1998), pp. 121–130, https://doi.org/10.1006/jcis.1998.5639.

[35] F. P. Medina and M. Peszynska, *Hybrid modeling and analysis of multicomponent adsorption with applications to coalbed methane*, in Porous Media: Theory, Properties, and Applications, Nova Science Publishers, Hauppauge, NY, 2016, pp. 1–52.

[36] F. P. Medina and M. Peszynska, *Stability for implicit-explicit schemes for non-equilibrium kinetic systems in weighted spaces with symmetrization*, J. Comput. Appl. Math., 328 (2018), pp. 216–231, https://doi.org/10.1016/j.cam.2017.07.020.

[37] A. Mielke, L. Paoli, A. Petrov, and U. Stefanelli, *Error estimates for space-time discretizations of a rate-independent variational inequality*, SIAM J. Numer. Anal., 48 (2010), pp. 1625–1646, https://doi.org/10.1137/090750238.

[38] P. A. Monson, *Recent progress in molecular modeling of adsorption and hysteresis in mesoporous materials*, Adsorption, 11 (2005), pp. 29–35, http://doi.org/10.1007/s10450-005-5894-7.

[39] R. H. Nochetto and G. Savaré, *Nonlinear evolution governed by accretive operators in Banach spaces: Error control and applications*, Math. Models Methods Appl. Sci., 16 (2006), pp. 439–477, https://doi.org/10.1142/S0218202506001224.

[40] R. H. Nochetto, G. Savaré, and C. Verdi, *A posteriori error estimates for variable time-step discretizations of nonlinear evolution equations*, Comm. Pure Appl. Math., 53 (2000), pp. 525–589.

[41] M. Peszynska, *A differential model of adsorption hysteresis with applications to chromatography*, in III Coloquio sobre Ecuaciones Diferenciales Y Aplicaciones, May 1997, J. G. Angel Domingo Rueda, ed., Vol. II, Universidad del Zulia, Maracaibo, Venezuela, 1998.

[42] M. Peszynska, *Methane in Subsurface: Mathematical Modeling and Computational Challenges*, IMA Vol. Math. Appl. 156, Computational Challenges in the Geosciences, C. Dawson and M. Gerritsen, eds., Springer, New York, 2013.

[43] M. Peszynska and R. E. Showalter, *Approximation of Hysteresis Functional*, manuscript to be submitted.

Downloaded 05/07/20 to 128.193.164.203. Redistribution subject to SIAM license or copyright; see http://www.siam.org/journals/ojsa.php

Copyright © by SIAM. Unauthorized reproduction of this article is prohibited.

[44] M. Peszynska and R. E. Showalter, *A transport model with adsorption hysteresis*, Differential Integral Equations, 11 (1998), pp. 327–340.

[45] B. K. Prusty, *Sorption of methane and CO_2 for enhanced coalbed methane recovery and carbon dioxide sequestration*, J. Nat. Gas Chem., 17 (2008), pp. 29–38, https://doi.org/10.1016/S1003-9953(08)60022-5.

[46] J. Rulla, *Error analysis for implicit approximations to solutions to Cauchy problems*, SIAM J. Numer. Anal., 33 (1996), pp. 68–87, https://doi.org/10.1137/0733005.

[47] J. Rulla and N. J. Walkington, *Optimal rates of convergence for degenerate parabolic problems in two dimensions*, SIAM J. Numer. Anal., 33 (1996), pp. 56–67, https://doi.org/10.1137/0733004.

[48] L. Sarkisov and P. A. Monson, *Hysteresis in Monte Carlo and molecular dynamics simulations of adsorption in porous materials*, Langmuir, 16 (2000), pp. 9857–9860, https://doi.org/10.1021/la001000f.

[49] B. Schweizer, *Hysteresis in porous media: Modelling and analysis*, Interfaces Free Bound., 19 (2017), pp. 417–447, https://doi.org/10.4171/IFB/388.

[50] C. J. Seto, G. T. Tang, K. Jessen, A. R. Kovscek, and F. M. Orr, *Adsorption Hysteresis and Its Effect on CO2 Sequestration and Enhanced Coalbed Methane Recovery*, AGU Fall Meeting Abstracts, (2006), D1542+.

[51] P. Shi and I. Babuška, *Analysis and computation of a cyclic plasticity model by aid of Ddassl*, Comput. Mech., 19 (1997), pp. 380–385, https://doi.org/10.1007/s004660050186.

[52] R. E. Showalter, *Monotone Operators in Banach Space and Nonlinear Partial Differential Equations*, Math. Surveys Monogr. 49, Amer. Math. Soc., Providence, RI, 1997.

[53] R. E. Showalter, T. D. Little, and U. Hornung, *Parabolic PDE with hysteresis*, Control Cybernet., 25 (1996), pp. 631–643, Distributed Parameter Systems: Modelling and Control (Warsaw, 1995).

[54] R. E. Showalter and X. Xu, *An approximate scalar conservation law from dynamics of gas absorption*, J. Differential Equations, 83 (1990), pp. 145–165.

[55] J. C. Simo and T. J. R. Hughes, *Computational Inelasticity*, Interdiscip. Appl. Math. 7, Springer-Verlag, New York, 1998.

[56] E. F. Toro, *Riemann Solvers and Numerical Methods for Fluid Dynamics*, 3rd ed., Springer-Verlag, Berlin, 2009, https://doi.org/10.1007/b79761; a practical introduction.

[57] J. A. Trangenstein, *Numerical Solution of Hyperbolic Partial Differential Equations*, Cambridge University Press, Cambridge, 2009; with 1 CD-ROM (Intel compatible PC or Mac).

[58] M. Ulbrich, *Semismooth Newton Methods for Variational Inequalities and Constrained Optimization Problems in Function Spaces*, MOS-SIAM Ser. Optim. 11, SIAM, Philadelphia, 2011.

[59] A. Visintin, *Differential Models of Hysteresis*, Appl. Math. Sci. 111, Springer-Verlag, Berlin, 1994.

[60] A. Visintin, *Quasilinear hyperbolic equations with hysteresis*, Ann. Inst. H. Poincaré Anal. Non Linéaire, 19 (2002), pp. 451–476, https://doi.org/10.1016/S0294-1449(01)00086-5.

[61] A. Visintin, *Quasilinear first-order PDEs with hysteresis*, J. Math. Anal. Appl., 312 (2005), pp. 401–419, https://doi.org/10.1016/j.jmaa.2005.03.048.

[62] H.-J. Woo, L. Sarkisov, and P.-A. Monson, *Understanding adsorption hysteresis in porous glasses and other mesoporous materials*, in Characterization of Porous Solids VI; Studies in Surface Science and Catalysis, Elsevier, The Netherlands, Vol. 144, 2002, pp. 155–162.

[63] J. Zhao, H. Xu, D. Tang, J. P. Mathews, S. Li, and S. Tao, *A comparative evaluation of coal specific surface area by CO_2 and N_2 adsorption and its influence on CH4 adsorption capacity at different pore sizes*, Fuel, 183 (2016), pp. 420–431.

[64] A. Zhezherun and D. Flynn, *ODEs with preisach operator under the derivative and with discontinuous in time right-hand side*, J. Phys. Conf. Ser., 55 (2006), pp. 232–242, https://doi.org/10.1088/1742-6596/55/1/021.

Downloaded 05/07/20 to 128.193.164.203. Redistribution subject to SIAM license or copyright; see http://www.siam.org/journals/ojsa.php

Copyright © by SIAM. Unauthorized reproduction of this article is prohibited.